

Figure 7-51. M/S and F/W Test vs. Analysis Linear Strain Comparisons at Location "A,"
Near Collar Insert, 3:00, 9:00 Position

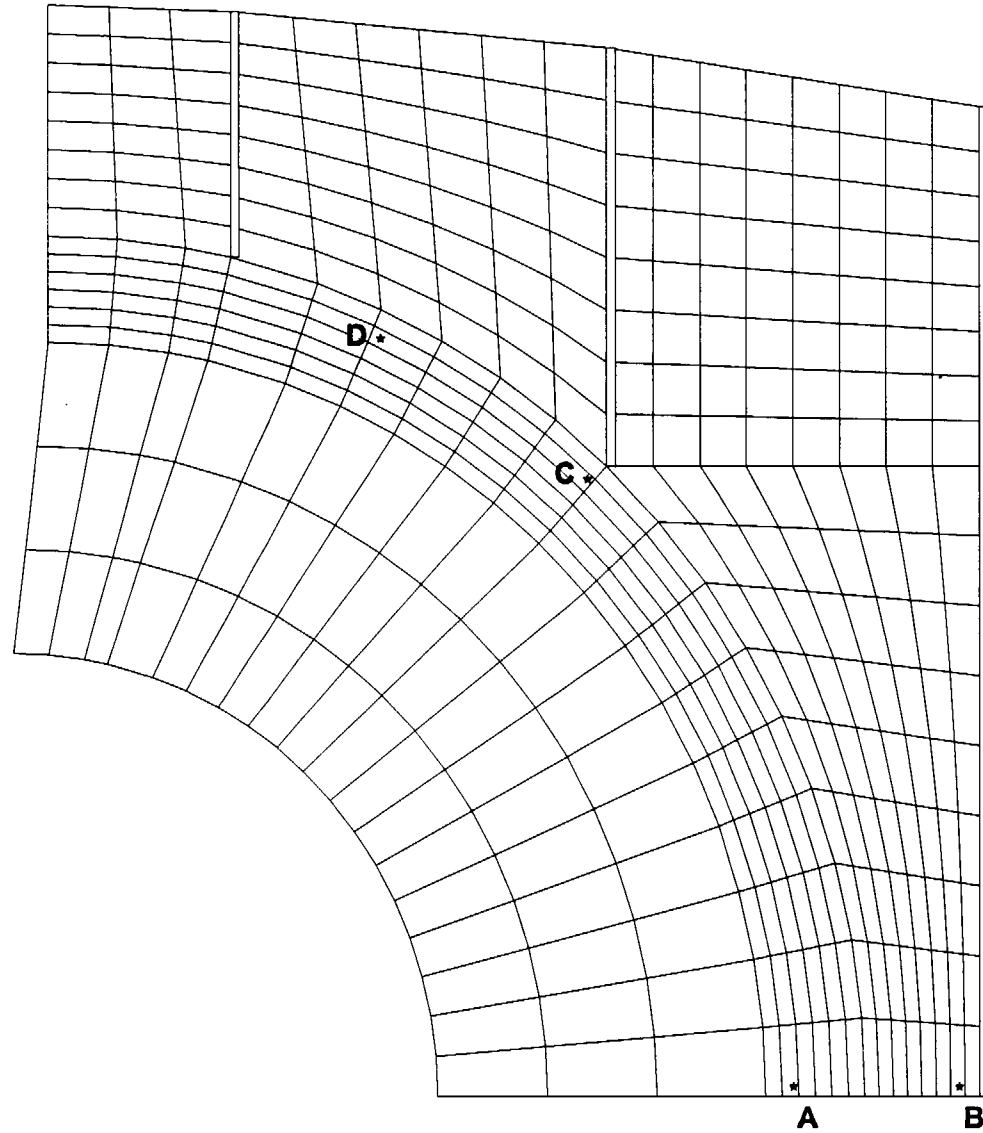


Figure 7-50. Liner Strain Locations for Comparing Analysis to M/S and F/W Gage Measurements

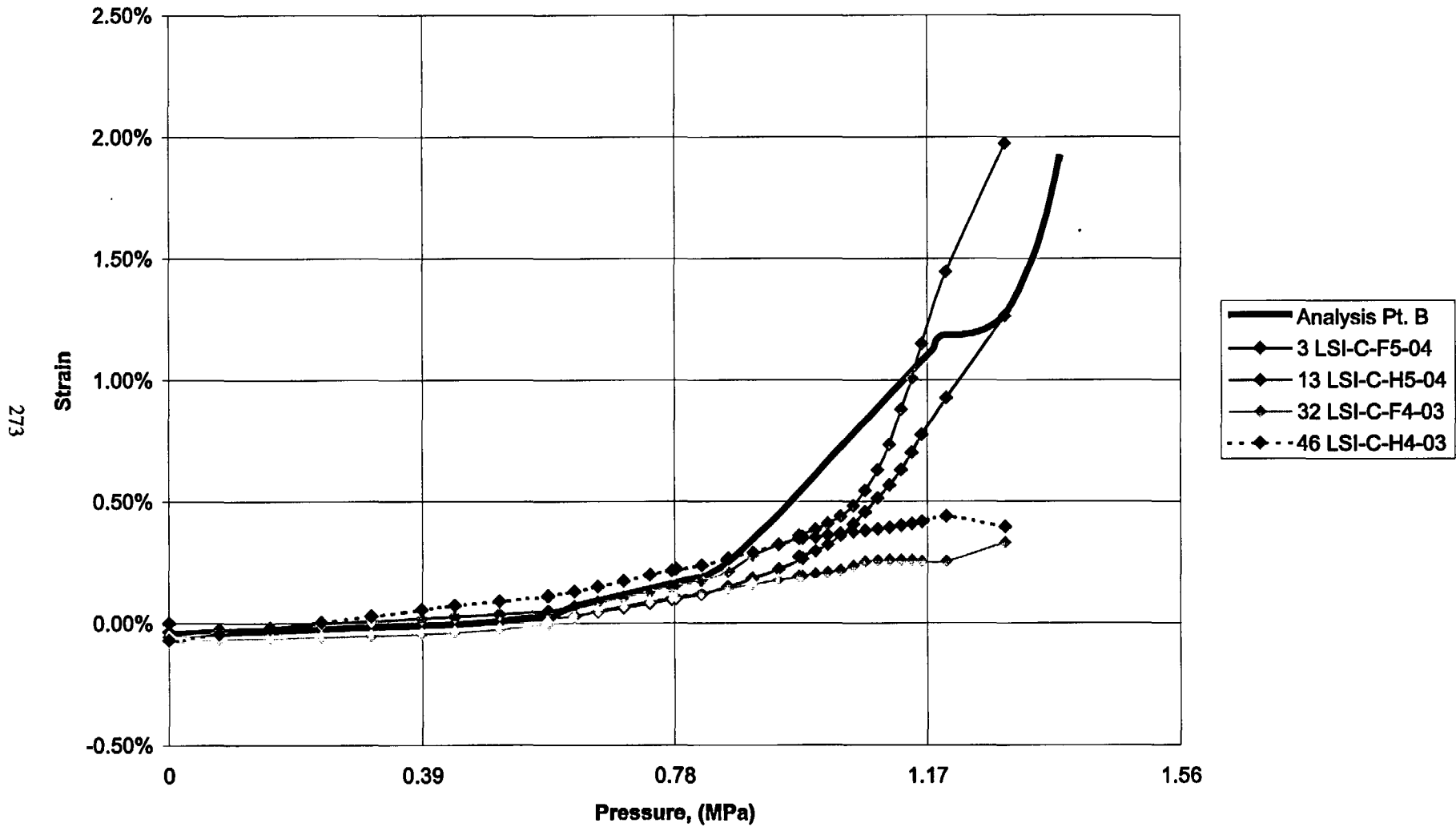


Figure 7-52. M/S and F/W Test vs. Analysis Linear Strain Comparisons at Location "B,"
Near T-Anchor, 3:00, 9:00 Position

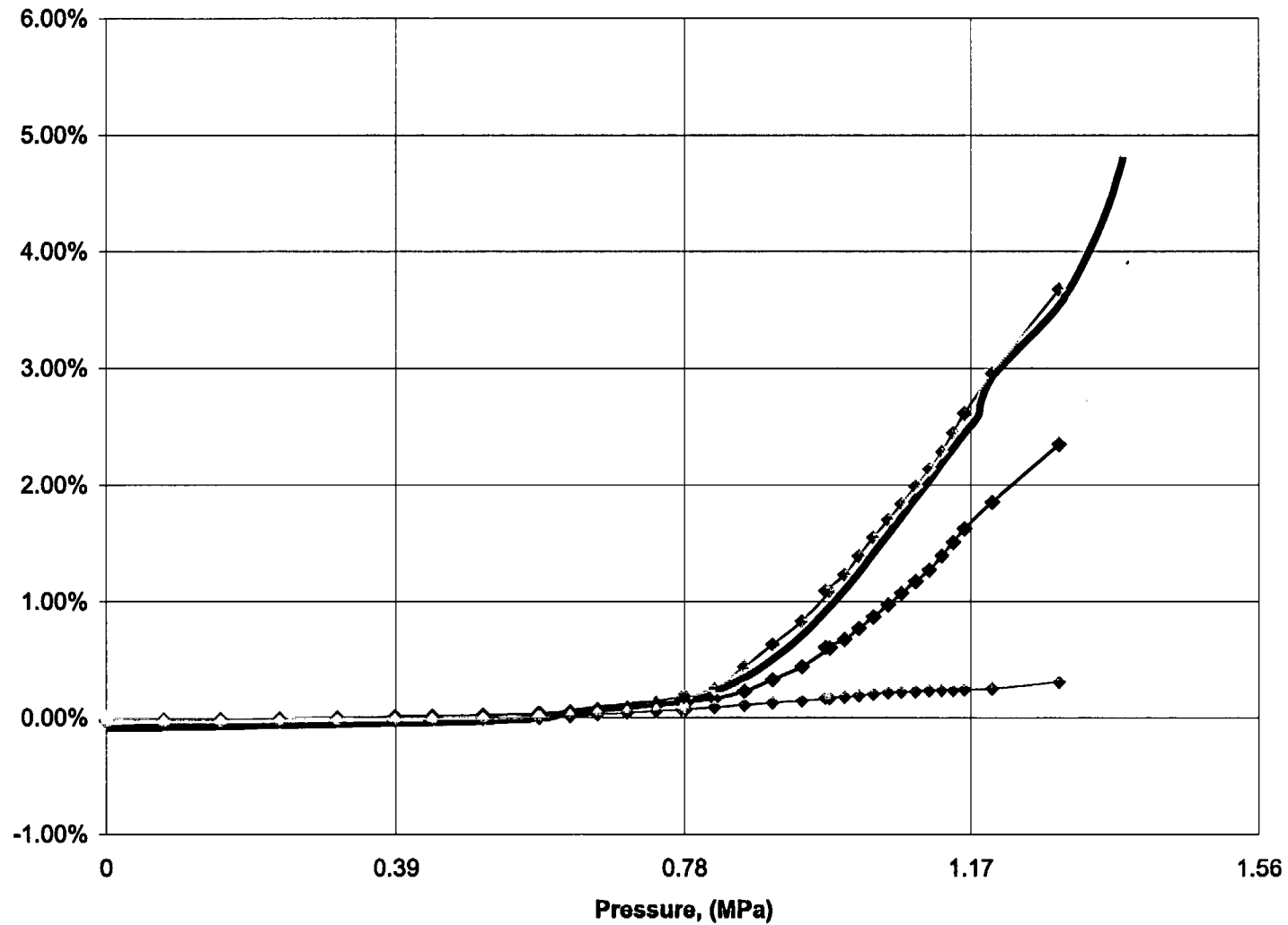


Figure 7-53. M/S and F/W Test vs. Analysis Linear Strain Comparisons at Location "C,"
Near T-Anchor, 3:00, 9:00 Position

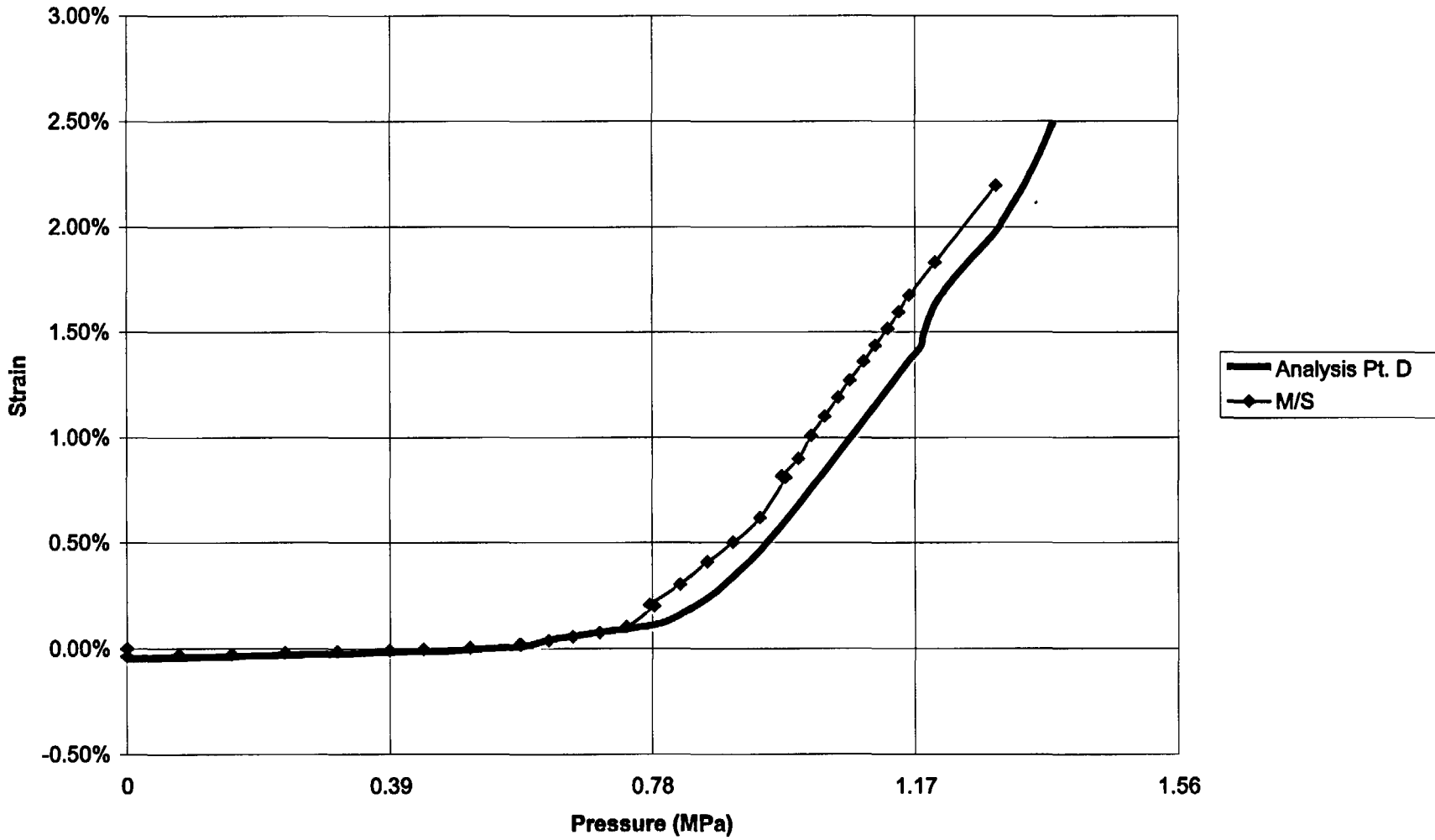


Figure 7-54. M/S Test vs. Analysis Linear Strain Comparisons at Location "D,"
Near Weld-Corner, 3:00, 9:00 Position.

8.0 LINER SEAM AND "RAT-HOLE" DETAIL ANALYSIS

8.1 Objectives of New Models

The PCCV model exhibited 16 distinct locations at which liner tears occurred. These locations are illustrated in Figure 8-1. In the pretest analysis report [1], the predicted elevated liner strain locations were categorized as Location Types 1 through 5.

1. Vertical weld seams intercepted by a horizontal stiffener and interrupted by rat-hole;
2. The termination points of vertical T-anchors near penetrations;
3. The termination points of horizontal stiffeners near penetrations;
4. Weld-connection points of multiple acute-angled liner pieces;
5. The wall-liner/basemat-liner connection.

Of these five, liner tears at the first three location types were predicted as likely to occur and Location 2 was identified as the most likely. However, all of the 16 tear locations observed were near weld seams, with some variation in the presence or configuration of a rat-hole. Furthermore, by comparing the "before and after" photos taken by SNL (Reference [8] with a typical tear, tear 16, shown in Figure 8-2), it is observed that liner welding irregularities were present at almost all of the tear locations. These irregularities included points of extensive repair, such as grinding, points of discontinuous or missing back-up bars, or points with weld and liner seam fit-up irregular geometry. Locations where a seam and rat-hole existed and high strains were measured, but a tear did not occur (e.g., at Location D-7, located just below where tear 16 occurred), further prove the importance of the welding details to the occurrence of liner tearing.

The liner weld irregularities have been well documented by the findings of [8], and are summarized as follows.

- Visual observation showed extensive grinding and weld repair in the liner welds where most of the tears occurred. Ultrasonic measurements showed substantial reductions in thickness near these tears. Measurements showed ~23% thickness reduction in many locations, and more (up to 40% in a few locations). (Several instances were found in which the liner adjacent to repair welds had been completely ground through and subsequently repair welded.)
- Localized plastic deformation occurred in association with many of the vertical field welds, particularly in the vicinity of the tears. No evidence of brittle fracture was seen.
- Photos of the back side of the liner revealed irregularities (missing segments of back-up bars, discontinuities in horizontal stiffeners) associated with a number of the tears.
- Mechanical testing showed only small strain localization in the weld heat affected zones — much less than observed in the liner base metal. Ultimate strength (~72 ksi) was not degraded by welding.
- No evidence was found of material problems that could account for the premature tearing of the liner. Only one tear (1) was associated with a weld defect. This was a lack-of-fusion defect, not porosity in the fusion zone.
- Metallography showed that nearly all of the tear areas had been ground at least 23%, both in preparation for repair welding and following repair welding. The report [8] concluded that most of the tears can be attributed to this excessive grinding.
- Some free-field tears were caused or exacerbated by back-side discontinuities in back-up bars and horizontal stiffeners. Some were also caused or exacerbated by back-side discontinuities (such as stiffeners) that served to localize plastic strain in these areas.

These observations, however, leave many unanswered questions about quantifying the effects of welding irregularities and distinguishing these from the strain concentration effects that are solely related to geometry.

In defining the objectives for posttest study of the liner tear locations, it is important that the study be aligned with the overall objectives of the containment research program; namely, to develop, refine, and validate analytical methods for predicting the overpressure behavior of containments. In other words, local analysis of the liner tear areas should not just model a detail where a tear occurred and see if the calculated high strains locations agree with the tear location, but should use the liner strain measurement data to refine and validate the methodology for modeling such locations. This, hopefully, will result in improved methods, and improved confidence in methods, for analyzing such details in full-scale containments. Further, by studying behavior with and without back-up bars, analytical support can be added to the test result conclusions already emerging from the SNL research about the importance of continuous back-up bar design code requirements. With these objectives in mind, the steps (and objectives) followed for this portion of the posttest analysis effort were as follows.

1. Analyze a "Type 1" liner strain concentration location at a group of liner strain gages to calibrate the finite element modeling to the strain measurements. The locations selected as typical were D-7 – near a typical vertical-seam/horizontal-stiffener-rathole – and tear 16, just a little above location D-7. Location D-7 is typical of rat-hole locations where significantly elevated strains occurred (some were measured), but no tears occurred. Tear 16 has some unique aspects, but part of the tear is typical of a number of tear geometries. The mesh is liner-only, without concrete.
2. Perform mesh-size and material property sensitivity analysis for calibrating to strain gage measurements to develop conclusions and guidelines for future modeling of similar details in full-scale containments. The material sensitivity analyses include the introduction of variation of stress-strain-curve assumptions for liner base metal, weld material, and heat-affected-zone material. It also includes differences in thickness from those of the nominal design, which were observed/measured on the as-built model. Input for these material property assumptions was obtained from SNL's metallurgical examination report [8].
3. Provide comparison to strain gage measurements.
4. Analyze with and without back-up bars.
5. Develop conclusions about the utility of local liner-only modeling for examining these type of details, and about the effects of liner base metal grinding, HAZ material property variation, and back-up bar discontinuities on the liner's propensity to tear.

8.2 Description of Computational Grids

The basic computational grid for the liner seam studies is shown in Figures 8-3 and 8-4. The grid consists of 4-node shell elements with reduced integration (ABAQUS S4R elements), and thicknesses assigned as described later in this chapter. Where unaffected by grinding, the as-measured thickness of 1.8 mm was used. Guidance for the thickness assignments was taken from SNL's posttest thickness measurements reported in [8]. The grids extend across one "span" between T-anchors, or 450 mm, on the assumption that between T-anchors, the liner is relatively free to locally strain and deform irrespective of the concrete backing. These grids also ignore the curvature of the PCCV wall, and so are flat.

The boundary conditions applied to the grids are a pinned condition at the left edge of the mesh and an applied x-displacement at the right edge.

The height of the model is 300 mm with hoop stiffeners at the 1/3 points. The lower stiffener has a rat-hole cutout at the midpoint. This mesh provides inherent comparisons between free-field liner behavior, liner vertical and horizontal seams without stiffeners, and a vertical seam with stiffener/rat-hole. It also specifically models the condition at Location D-7, and by adding various flaws (described later), it can be made to simulate tear 16 and other rat-hole locations, with or without back-up bars.

All edges of the grids have fixed conditions for out-of-plane deformations and rotational degrees of freedom. Horizontal (hoop) and vertical (meridional) displacements are fixed along the left and bottom edges, respectively. The grids are loaded in displacement control horizontally and vertically along the right and top edges. Loading in both the hoop and

meridional directions simulates the bi-axial states of stress developed in the actual containment liner. The load history applied was derived from LST data. The applied vertical displacement was calculated from the liner meridional strain, measured at gage LSI-M-Z6-01, multiplied by the model height, 300 mm. The history of liner meridional strain and the best-fit curve used for the model is shown in Figure 8-5. The horizontal displacement history was derived from the radial displacement, measured at gage DT-R-Z5-01. The radial displacement was converted to hoop strain by dividing by the radius, 5373 mm, and then multiplying by the mesh width, 450.4 mm. Figure 8-6 shows the radial displacement history and the best-fit curve used for the analysis.

The model (and most of its variations) was loaded from an equivalent internal pressure of 0.55 MPa (80 psig) up to the end of the LST, 1.30 MPa (187.9 psig) or 3.3 Pd. The starting pressure was chosen as the point where the internal pressure overcomes the initial containment prestressing when the hoop strain is approximately zero. Table 8-1 lists the measured liner strain and displacement and the converted data for the displacement boundary conditions. Temperature correction was not applied. Two of the parameter runs (the ones most closely replicating Location D-7), were then run beyond 3.3 Pd to see when a tear might have occurred if the LST had proceeded to higher pressure.

Table 8-1. Liner Model Displacement Loading Boundary Conditions (for LST)

Pressure MPa	Radial Disp. mm (estimated)	Meridional Strain (estimated)	Δ horizontal (mm)	Δ vertical (mm)
0.55	-0.35	-0.00023	-0.0305	-0.0711
85.0	0.43	-0.00022	0.0014	-0.0026
90.0	1.14	-0.00021	0.0038	-0.0025
95.0	1.87	-0.00020	0.0062	-0.0024
100.0	2.58	-0.00019	0.0085	-0.0023
105.0	3.25	-0.00018	0.0107	-0.0022
110.0	3.90	-0.00017	0.0129	-0.0020
115.0	4.53	-0.00016	0.0149	-0.0019
120.0	5.17	-0.00015	0.0171	-0.0018
125.0	5.77	-0.00014	0.0190	-0.0016
130.0	6.40	-0.00012	0.0211	-0.0015
135.0	7.08	-0.00010	0.0234	-0.0012
140.0	7.77	-0.00008	0.0256	-0.0010
145.0	8.54	-0.00006	0.0282	-0.0007
150.0	9.35	-0.00004	0.0308	-0.0004
155.0	10.30	-0.00001	0.0340	-0.0002
160.0	11.27	0.00002	0.0375	0.0003
165.0	12.60	0.00010	0.0416	0.0011
170.0	14.00	0.00017	0.0462	0.0020
175.0	15.65	0.00024	0.0516	0.0028
180.0	17.50	0.00032	0.0577	0.0038
185.0	19.70	0.00042	0.0650	0.0050
187.9	21.15	0.00048	0.0698	0.0057

8.3 Mesh Sensitivity Study

Three variations of the mesh refinement were investigated in the initial parameter study. Figures 8-7 – 8-9 show the finite element grids used as the baseline, coarse, and fine models, respectively. The coarse mesh has approximately half the refinement of the baseline model and the fine mesh has approximately double the refinement. The number of nodes, elements, and degrees of freedom for each model are summarized in Table 8-2.

Table 8-2. Liner Model, Mesh Sensitivity, Model Statistics

Model	Coarse	Baseline	Fine
Number of Nodes	11011	20724	33391
Number of Elements	10428	19960	32436
Number of D. O. F.	64956	123006	198720
Percent Difference, Baseline	-47%		62%

Maximum principal strain contour plots of the liner for the baseline, coarse, and fine models are shown in Figures 8-10 – 8-12 at the end of the analysis, approximately 187.9 psig. The local contour plots of the liner in the stiffener cutout location have equal widths and heights between the three different grids. The dimensions with respect to the weld centerline and the stiffener centerline are shown on each plot. These results show similar response with strain concentrations developing at the reentrant corners of the rat-hole and liner. As expected, the peak strains at the concentration vary somewhat, with the largest strain calculated for the finest mesh. The peak strains at the reentrant corner are 7.1%, 10.2%, and 13.0% for the coarse, baseline, and fine grids, respectively.

To more accurately compare the sensitivity of the mesh refinement, strains at locations away from the concentration were extracted. Figures 8-13 and 8-14 show plots of the principal strain history for the three models at locations approximately 5 mm and 1.2 mm below the stiffener reentrant corner. These comparisons show a significant change in strain histories between the course mesh and baseline mesh, but much closer comparison between baseline and fine. Figures 8-15 and 8-16 show strain profiles in line with the stiffener, moving across the rat-hole. To compare strains at the same geometric positions, two integration points of the fine mesh were averaged to provide data comparisons at a single point of the baseline mesh. This shows that by simple averaging of strains across a single element, the fine and baseline meshes produce roughly the same results. Thus it was concluded, in the analyst's opinion, that the baseline mesh discretization is of adequate size for the liner tear study. Note that the fundamental element dimension (hoop direction) for the baseline mesh was 0.8 mm, a little less than half of the liner thickness, and about half of the reduced liner thickness.

8.4 Material and Geometry Variations

The next phase of the liner tear study conducted analyses to assess the effects of material and geometry variations. The first variation was to implement varying material properties near the weld areas. This included assignment of different material properties to the base metal, HAZ, and weld fusion zone (WFZ) regions of the model. The second variation only modified the material in the WFZ. This is expected to show that strain localization develops predominately at softer HAZ, as opposed to the discontinuity immediately adjacent to the WFZ. The final phase incorporated geometry modifications to the model near the weld lines. This included thinning elements and varying the extent of thinning in the vicinity of the welds due to grinding. The geometry modifications were coupled with modified material properties ranging from uniform to including variations of base metal, HAZ, and WFZ regions. The material and geometry variations were based on data contained in the SNL metallurgical analysis report [7]. The material property parameters from [7] are summarized in Table 8-3.

Description of the variations introduced for the parameter study are provided below, listed in Table 8-4, and illustrated in Figure 8-17. The material variations were introduced by shifting the entire plastic portion of the stress-strain curve up or down by the ratio of the UTS listed in Table 8-3 to the UTS of the base metal listed in Table 8-3.

8.4.1 Mesh Sensitivity Study

1. Baseline Mesh
2. Coarse Mesh
3. Fine Mesh

All subsequent models use the baseline mesh.

Table 8-3. Microhardnesses of Zones Surrounding Welds (from Reg. [8])

Zone	Avg. Hardness*	Std. Dev.	UTS (ksi)**	UTS (MPa)**
Base metal	160	6.9	74.5	515
Fine-grained HAZ	151	4.3	71	490
Med-grained HAZ	154	3.4	72	495
Coarse HAZ	164	6.8	76.5	525
Fusion Zone	180	11.4	84	580
Recrystallized fusion zone	173	5.9	80.5	550

* Vickers hardness, 100 gram load

** Ultimate Tensile Strength (UTS) estimates. Reference [8] notes that UTS estimates are based on conversion tables for hardness tests made with much heavier loads. As a result, the estimated UTS values should be taken only as approximations; they are useful primarily for comparing the expected relative strengths of the various regions, not the absolute strengths.

8.4.2 Material Variation

1. Varying material, base metal, fine, medium, coarse HAZ regions, and fusion zones.
2. Varying material, base metal, and fusion zones. No HAZ material variation.

8.4.3 Geometry and Material Variation

1. Varying material, base metal, fine, medium, coarse HAZ regions, and fusion zones. Grinding from base to horizontal seam weld, Extent +/- 10mm either side of vertical seam weld, 20% thickness reduction.
2. Varying material, base metal, fine, medium, coarse HAZ regions, and fusion zones. Grinding from base to horizontal seam weld, Extent +/- 20 mm either side of vertical seam weld, 20% thickness reduction.
3. Varying material, base metal, and fusion zones. Grinding from base to horizontal seam weld, Extent +/-10 mm either side of vertical seam weld, 20% thickness reduction.
4. Varying material, base metal, and fusion zones. Grinding from base to horizontal seam weld, Extent +/-20 mm either side of vertical seam weld, 20% thickness reduction.
5. Varying material, base metal, fine, medium, coarse HAZ regions, and fusion zones. Grinding from base to horizontal seam weld, Extent +/- 10mm either side of vertical seam weld, 40% thickness reduction.
6. Varying material, base metal, fine, medium, coarse HAZ regions, and fusion zones. Grinding from base to horizontal seam weld, Extent +/- 20 mm either side of vertical seam weld, 40% thickness reduction.
7. Varying material, base metal, and fusion zones. Grinding from base to horizontal seam weld, Extent +/- mm either side of vertical seam weld, 40% thickness reduction.
8. Varying material, base metal, and fusion zones. Grinding from base to horizontal seam weld, extent +/- 20 mm either side of vertical seam weld, 40% thickness reduction.

8.5 Results and Comparisons with Test

The spatial distributions of stresses and strains at a pressure of 188 psig (3.3 Pd) for the baseline plus the first 10 parameter cases (Cases 1 and 4 through 13) are shown in Figures 8-18 through 8-39. Each set provides horizontal

Table 8-4. Sensitivity Study Parameters

Analysis	Overgrinding Width (mm)	Base Metal			Fine Grained HAZ			Medium Grained HAZ			Coarse Grained HAZ			Fusion Zone		
		K	σ_y (ksi)	t (mm)	K	σ_y (ksi)	t (mm)	K	σ_y (ksi)	t (mm)	K	σ_y (ksi)	t (mm)	K	σ_y (ksi)	t (mm)
b-01	0.0	1.00	54.56	1.80	1.00	54.56	1.80	1.00	54.56	1.80	1.00	54.56	1.80	1.00	54.56	1.80
b-02*	0.0	1.00	54.56	1.80	1.00	54.56	1.80	1.00	54.56	1.80	1.00	54.56	1.80	1.00	54.56	1.80
b-03**	0.0	1.00	54.56	1.80	1.00	54.56	1.80	1.00	54.56	1.80	1.00	54.56	1.80	1.00	54.56	1.80
b-04***	0.0	1.00	54.56	1.80	0.95	51.83	1.80	0.97	52.92	1.80	1.03	56.20	1.80	1.13	61.65	1.80
b-05	0.0	1.00	54.56	1.80	1.00	54.56	1.80	1.00	54.56	1.80	1.00	54.56	1.80	1.13	61.65	1.80
b-06	10.0	1.00	54.56	1.44	0.95	51.83	1.44	0.97	52.92	1.44	1.03	56.20	1.44	1.13	61.65	1.80
b-07	20.0	1.00	54.56	1.44	0.95	51.83	1.44	0.97	52.92	1.44	1.03	56.20	1.44	1.13	61.65	1.80
b-08	10.0	1.00	54.56	1.44	1.00	54.56	1.44	1.00	54.56	1.44	1.00	54.56	1.44	1.13	61.65	1.80
b-09	20.0	1.00	54.56	1.44	1.00	54.56	1.44	1.00	54.56	1.44	1.00	54.56	1.44	1.13	61.65	1.80
b-10	10.0	1.00	54.56	0.99	0.95	51.83	0.99	0.97	52.92	0.99	1.03	56.20	0.99	1.13	61.65	1.80
b-11	20.0	1.00	54.56	0.99	0.95	51.83	0.99	0.97	52.92	0.99	1.03	56.20	0.99	1.13	61.65	1.80
b-12	10.0	1.00	54.56	0.99	1.00	54.56	0.99	1.00	54.56	0.99	1.00	54.56	0.99	1.13	61.65	1.80
b-13	20.0	1.00	54.56	0.99	1.00	54.56	0.99	1.00	54.56	0.99	1.00	54.56	0.99	1.13	61.65	1.80
c-03	With back-up bars and Tear 16 modeling (missing short section of back-up bar on horiz. weld seam)															
c-04	With back-up bars and Tear 16 modeling variation (added "over" liner grinding only at missing horiz. back-up bar)															
c-05	With back-up bars and Tear 16 modeling															
c-06	With back-up bars; no Tear 16 modeling															
c-07	With back-up bars, and additional grinding only at "Tear 16"; no missing back-up bar															

- * 2 is coarse mesh
- ** 3 is fine mesh
- *** 4 is baseline mesh (best estimate case)

(hoop) stress, vertical (meridional) stress, and Von Mises stress, and the analogous strain components. The figures illustrate competing strain concentrations and provide evidence of the variety of conditions that probably existed in the PCCV model (both at the tear locations and at similar details that didn't tear). It is clear from Figures 8-18 through 8-25 (Cases 1, 4, 5, 6) that the cases with unmodified thicknesses all develop their highest strains near the stiffener edge, not next to the weld. Further, for Cases 1 and 4, the end of the analyses (which corresponds to 3.3 Pd and the end of the LST) show peak strains lower than the tearing threshold. (Depending on the biaxiality of stress, the tearing threshold is calculated to be approximately 20%. The liner tearing criteria is covered in detail in the pretest analysis report, and not repeated here.) The baseline case peak effective plastic strain reaches only 11.4%, so for a "perfectly" constructed detail, the model analyzed here does not predict a tear. When the best estimated HAZ and fusion zone material strengths are introduced (Case 4), some strain elevation moves into the fine HAZ, but it is not as large as the strain at the stiffener edges and the peak strain (18.7%) is still just below the strain that would indicate occurrence of a tear. This agrees with the observed behavior at locations like D-7.

When only the fusion zone strength is elevated, (Case 5), the level of strain concentration at the stiffener edges is intensified, and strains reach 21%, which is likely a tear condition. Since this was not observed in the test at locations without grinding related thickness reductions, it is probably not a realistic case; i.e., the best estimate material property adjustments appear necessary to achieve the most realistic behavior prediction.

When 20% thickness reductions are introduced (Cases 6 and 7) with best estimate weld zone strengths, the case with 20 mm of grinding width reaches its highest strains at the stiffener edge ($\max \epsilon_{\text{eff}} = 17.8\%$), while the Case with 20 mm grinding width shows much more widely distributed elevated strains and also no fracture ($\max \epsilon_{\text{eff}} = 12.2\%$). When only the grinding is introduced with no change to material properties (Cases 8 and 9), the high strain zone moves completely away from the stiffener ends and concentrates itself in the thinned area. But neither of these cases reach fracture.

In the last set of cases without back-up bars, 10 through 13, the thinning is 40%, and the highest elevated strains generally move into the thinned area. Cases 10 and 12 (23% and 20% strains) certainly fracture, while Case 11 and 13 (11% and 16% strains) do not. These Cases are particularly interesting, and in fact, for the tear locations that tore immediately adjacent to a vertical weld (Case 10), with its very focused band of high strain next to the fusion zone, appears to provide a good simulation of the tearing phenomena. All of these results are summarized in Table 8-5. This table also provides author's opinions as to whether the specific model variation captures observed behavior on the model, and where. These opinions are supported later in the discussion.

The next plot series, Figure 8-41 through 8-52, show horizontal (hoop) and vertical (meridional) strains at selected locations identified in Figure 8-40. The cases with modified material properties (4, 6, 7, 10, 11) are compared to the baseline on the left, and without modified material properties (5, 8, 9, 12, 13) are compared to the baseline on the right.

In order to draw conclusions about modeling such details, some comparisons with gage measurements are provided in Figures 8-54 through 8-58. In each plot, the gage name is provided, and the position numbers from the FE analysis are mapped in Figure 8-53. The gages are taken from various locations on the model that are all near vertical weld seams and rat-hole stiffener details: namely, at locations A5, K5, J5, D7, and Z5. A5 is near the edge of the E/H embossment that exhibited tears, and K5 is on the other side, which did not tear. J5 is near the 270° buttress, and D7 is near the 0° buttress. Z5 is near the 135 degree azimuth.

Fair correlation is obtained at position 2 (fine grained HAZ, near weld, in line with stiffener) with Cases 7 and 9. Case 10 agrees well below 3 Pd, but then turns up too quickly. Position 4 also shows fair correlation with several of the cases, and position 5 appears to agree with Cases 10 and 12.

8.6 Back-Up Bars and Additional Analyses

Since these models provide a reasonable representation of the actual liner behavior, a few models were extended to develop further insights. Because some locations (and some FE models that simulate them) clearly do not develop tears, the first model extension was to predict when these non-tear rat-hole details might have torn, had the LST proceeded to higher pressure. For this, Cases 1 and 4 were extended to higher pressure; of course, this was only a hypothetical simulation. Case 1 was chosen because it is the baseline, and Case 4 was chosen as a best estimate simulation of pristine

rat-hole details that did not tear, possibly similar to Locations D-7, Z-5, and J-5. The displacement versus pressure extension was made using the SFMT. Data from the SFMT at radial displacement gage DT-R-Z5-D1 was obtained and added to the LST data, as shown in Figure 8-59. The vertical boundary condition was created by a curve-fit extrapolation (Figure 8-60), because no liner strain measurements were taken in the SFMT.

The stress and strain contour results are plotted at 3.4 Pd and 3.6 Pd in Figures 8-61 and 8-68. They indicate a prediction that either case (with or without the HAZ material modifications) would tear prior to reaching 3.4 Pd. The tear, indicated by $\epsilon_{\text{eff}} = 26.3\%$, would occur next to the stiffener end. The strain histories of the element locations shown in Figure 8-40 for these extension runs are shown in Figures 8-69 through 8-76. These provide further evidence on which to base the prediction of tearing pressure, pegging it to between 3.37 and 3.4 Pd. These two cases are entitled Case 1b and 4b, because they use the same models as Case 1 and 4 – just pushed to higher pressure.

The next extension of the parametric study series added back-up bars and more specifically captured the details at tear 16. This set of changes is illustrated in Figure 8-77. The back-up bars are extra, separate elements. The back-up bar elements were only joined to the liner at the edges of the fusion zone, so they did not strengthen the liner in areas of liner thinning/grinding.

Tear 16 is of particular interest for this study because it encompasses three types of tear mechanisms along the path of the tear:

1. Across a horizontal seam where a short stretch of back-up bar was ground off (and with possible liner thinning caused by the grinding);
2. Along the HAZ next to a vertical seam; and
3. Next to the edge of the vertical back-up bar or next to the stiffener end inside the rat-hole.

Models C3, C4, C5, C6, and C7 capture possible variations of geometry that could influence these tearing mechanisms. The grinding and back-up bar versions are illustrated in Figure 8-77 and in Table 8-5. The stress strain contours for these models (at 3.3 Pd) are shown in Figures 8-78 through 8-87. Strain history plots versus pressure are also shown in Figures 8-89 through 8-94, the locations of which are shown in Figure 8-88.

As described previously, the conclusions of the studies are summarized in Table 8-5. The results are all tabulated at $P=188$ psig, 3.3 Pd. Many of the conclusions were based on comparisons to:

- Strain gage measurements,
- Physical measurements of liner ground thickness and HAZ characteristics obtained from [7], and
- Visual observations of tear geometry

The geometric locations of the gage groups are shown in Figures 8-95 through 8-98. Many detailed strain gage comparisons were developed at the pressure snapshots of 2.8 Pd and 3.3 Pd. Gage readings are compared to contour illustrations in Figures 8-99 through 8-114. These compare the gage readings for the five rat-hole gage groups directly on the same plots. Thus, one or more gage groups may agree well with a contour while other gage groups may not. The gage group's "agreement" is summarized in Table 8-5.

8.7 Conclusions of Liner Seam Analyses

The conclusions of the liner seam/rat-hole modeling study are summarized below.

- By comparison with strain gage measurements and posttest liner tear observations, some of the finite element liner-only meshes capture the strain concentrations in and around the rat-holes and liner welds reasonably well.

- Because of competing mechanisms (between the weld zone and the ends of stiffeners), making yield and ultimate strength adjustments to the HAZ material properties appears to be justified and necessary to correctly predict strain concentration location and intensity.
- Case C6 with back-up bars, nominal geometric properties, and best-estimate material properties is the best predictor of defect-free construction of rat-hole/weld-seam details, as probably occurred in the PCCV model at locations such as D7 and J5; however, even without back-up bars, Case 4, also provides reasonable simulation (and correlation with gages) at these locations.
- Case 10 appears to provide the best simulation of the behavior of tear occurrences in which severe liner thinning (due to weld repair grinding) was present and back-up bars were absent; these conditions existed at tears 7, 8, 10, 12, 13, 14, 15, and 16.
- Case C5 showed the highest strains of all the cases (with a peak over twice as high as Case 10) even though it is analogous to Case 10, with back-up bars added. This shows that in the presence of grinding-caused liner thinning, back-up bars may actually exacerbate the strain concentration in the HAZ. Note, however, that the peak strain in the HAZ was also strongly exacerbated by the presence of the tear 16 detail. This case appears to reasonably simulate the tears that occurred *with* back-up bars present, namely, tears 1, 2, 6, 9, 11, and 16. The severity of the strain in this case also shows that a tear ($\epsilon_{eff} > 20\%$) at the geometry simulated would have been predicted to occur as early as 3.0 Pd.
- Cases C3 and C4 reasonably simulate tear 16. The lower strain concentration in these models also simulate other tears that appear to have formed at the ends of stiffeners: tears 3, 6, 7, 9, and 11.
- If a section of liner with a rat-hole/liner-seam detail such as that at tear locations 7, 12, 13, and 15 is subjected to additionally elevated strain (i.e. strain across the liner model that is larger than free-field global strain), a tear even earlier than 3.0 Pd can be justified. In practice, such a prediction could be approximated using a strain concentration factor approach. The strain concentration factors ($K = \text{peak } \epsilon_{eff} \text{ divided by global } \epsilon_{hoop}$) implied by this liner seam study are as follows:

$$\epsilon_{hoop} = 21\text{mm}/5375\text{mm} = 0.00391$$

Case 4:	K = 48 (tear at stiffener end, no back-up bar)
Case C6:	K = 45 (tear at stiffener end, with back-up bar)
Case 10:	K = 59 (tear at HAZ, no back-up bar, and 40% thickness reduction due to grinding)
Case C4:	K = 91 (tear at tear 16, if a short segment of horizontal weld seam back-up bar is missing)

- Using the LST pressurization, the rat-hole/seam locations without defects, such as location D-7, still would have developed liner tears by a pressure of 3.4 Pd.

Table 8-5. Peak Effective Plastic Strains for Each Case

Case	Material	Grinding	Back-up Bars	Tear 16 Detail	Peak Strain at 188 psig (3.3 Pd)		Tear Predicted	Behavior Similar to:
					Location	Max. Effective Strain		
1	Nominal	No	No	--	Stiffener End	0.114	No	None
4	Heat-Adjacent	No	No	--	"	0.187	No	Yes-D7, Z5, A5, J5
5	Nominal+F.Z.	No	No	--	"	0.213	Yes	None
6	Heat-Adjacent	20% - 10mm	No	--	"	0.178	No	Yes-D7, K5
7	Heat-Adjacent	20% - 20mm	No	--	Stiffener End/Fine HAZ	0.122	No	Yes-D7, K5
8	Nominal+F.Z.	20% - 10mm	No	--	10mm from weld	0.121	No	Yes-D7, K5
9	Nominal+F.Z.	20% - 20mm	No	--	Stiffener End	0.164	No	None
10	Heat-Adjacent	40% - 10mm	No	--	Fine HAZ	0.231	Yes	Yes-tear 1,7,8,10, 12,13,14,15, 16
11	Heat-Adjacent	40% - 20mm	No	--	Stiffener End/Fine HAZ	0.107	No	Yes-K5, D7
12	Nominal+F.Z.	40%-10mm	No	--	10mm from weld	0.199	Yes	No
13	Nominal+F.Z.	40% - 20mm	No	--	Stiffener End	0.157	No	Yes-K5, D7
C3	Heat-Adjacent	No	Yes	Yes	At tear 16 (and Stiffener End)	0.361	Yes/Yes	Yes-D7*, tear 3,6,7,9, 11,16
C4	Heat-Adjacent	No	Yes	Yes w/ grinding	Stiffener End (and tear 16)	0.354	Yes/Yes	Same as C3
C5	Heat-Adjacent	40% - 10mm	Yes	Yes w/ grinding	Fine HAZ (and tear 16)	0.567	Yes/Yes	Yes-D7*, tear 1,2,6,9, 11,16
C6	Heat-Adjacent	No	Yes	No	Stiffener End	0.175	No	Yes-D7, J5 A5
C7	Heat-Adjacent	No	Yes	No w/ Grinding	Stiffener End	0.299	Yes	Yes-tear 3,6,9,11

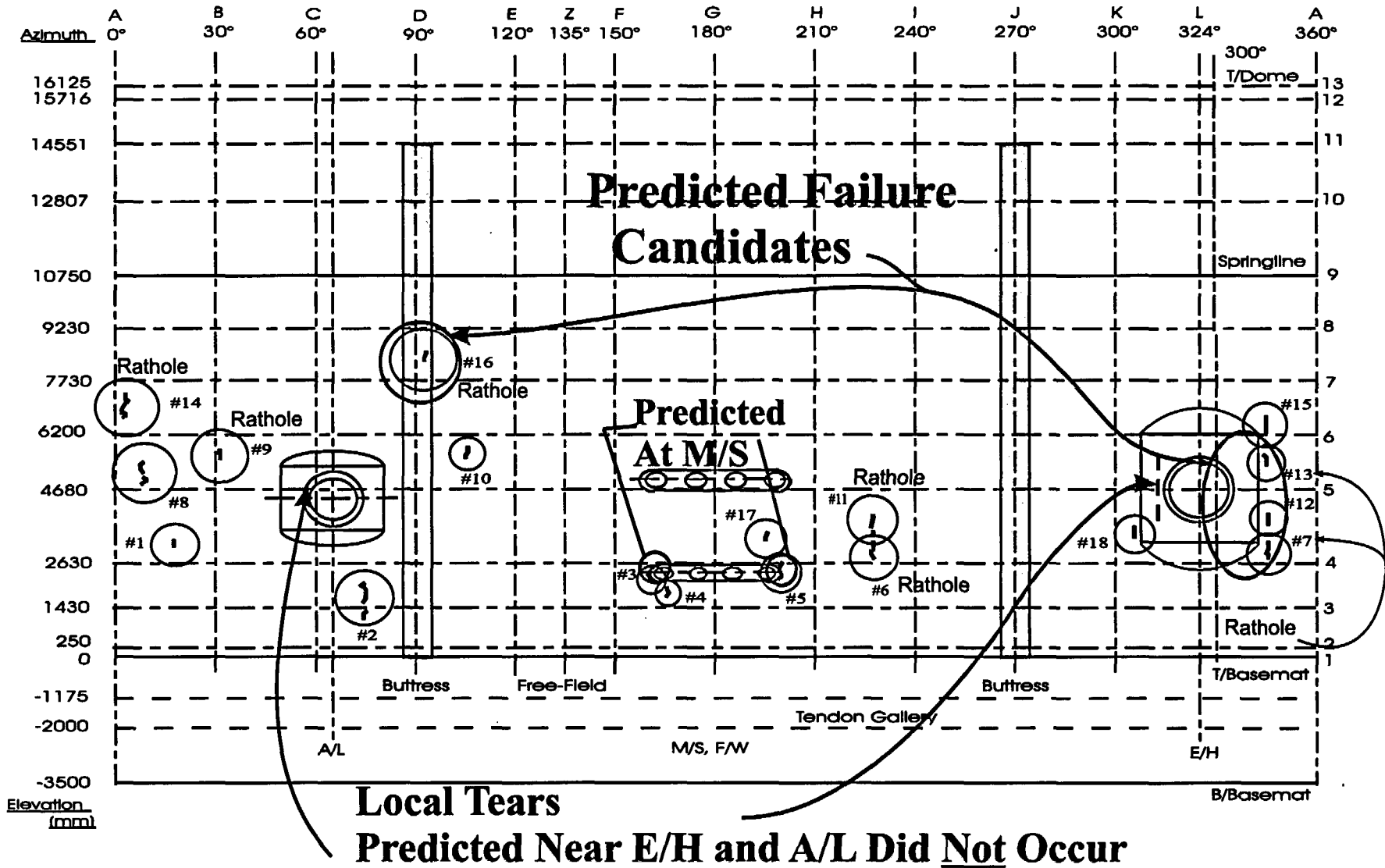
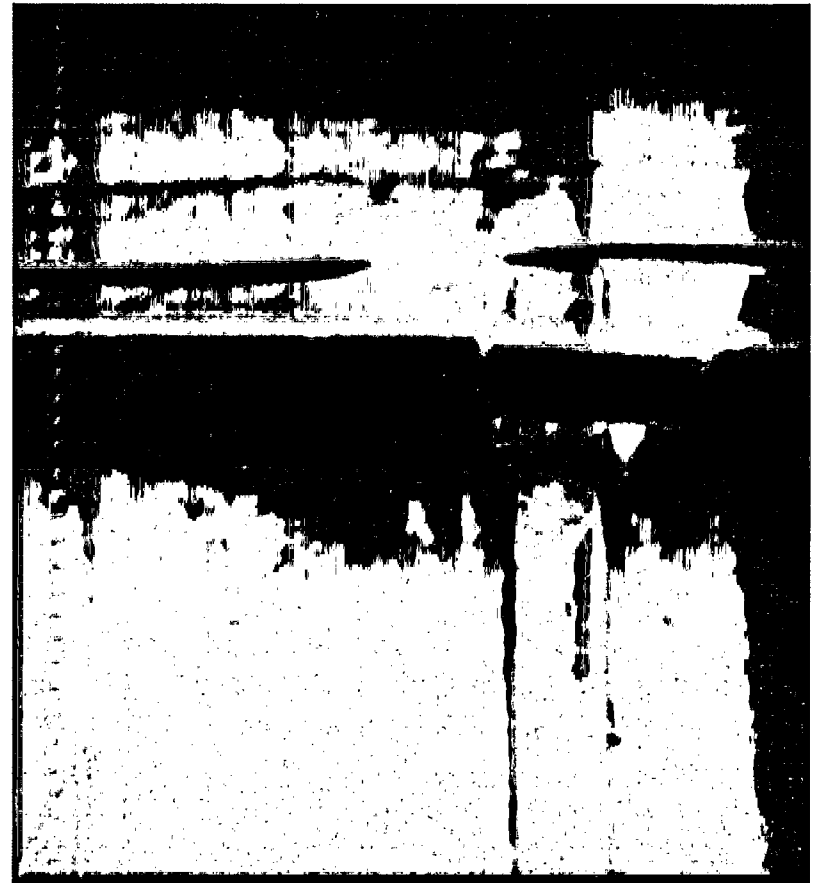
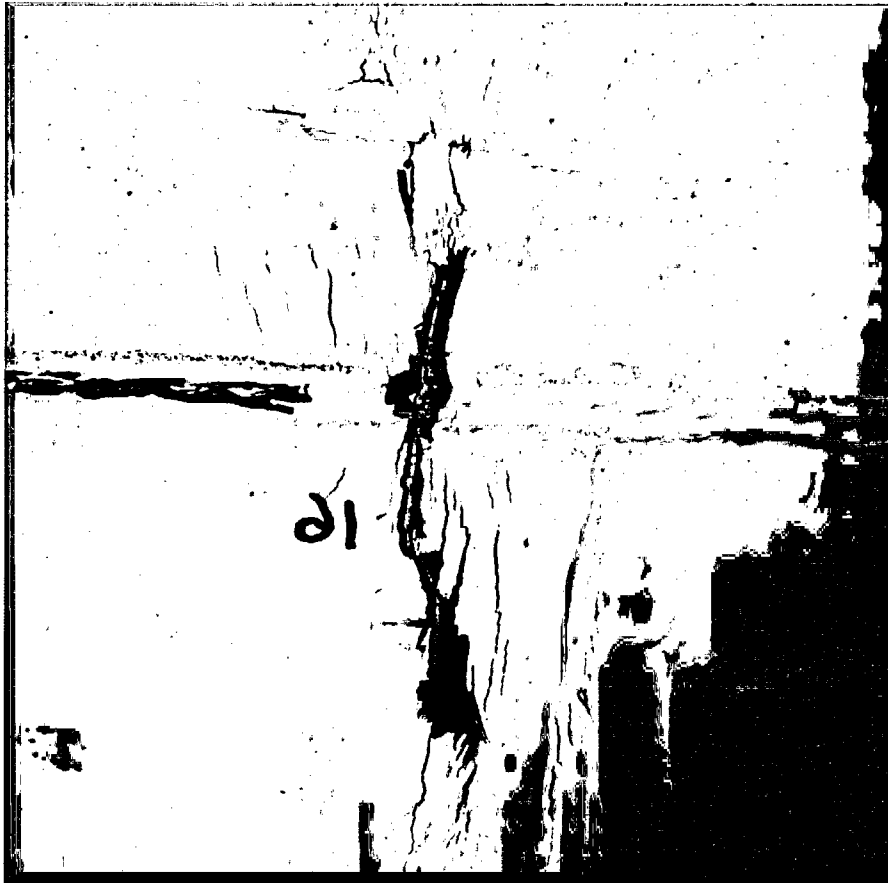


Figure 8-1. Liner Tears Observed in the 1:4 Scale PCCV LST

Liner Tear #16



(Image reversed for comparison)

Figure 8-2. Photos of Typical Liner Tear, Inside Surface (Left), Concrete Side (Right)

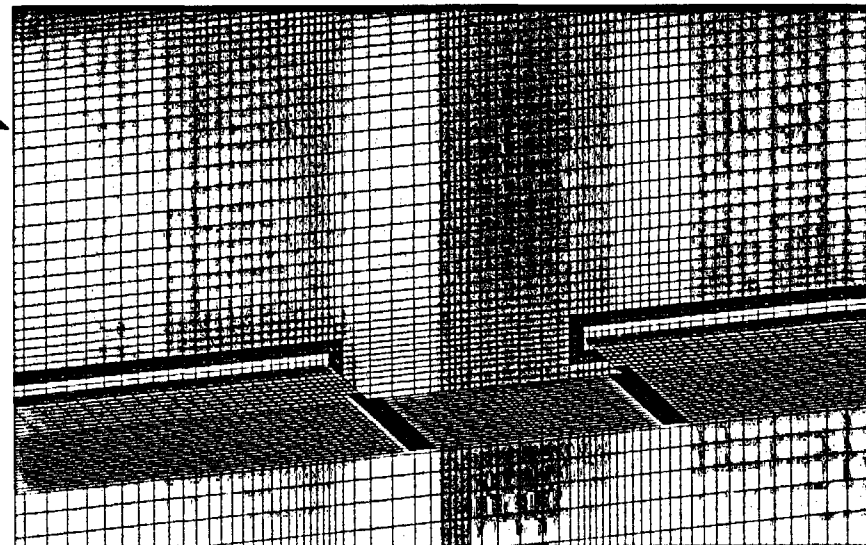
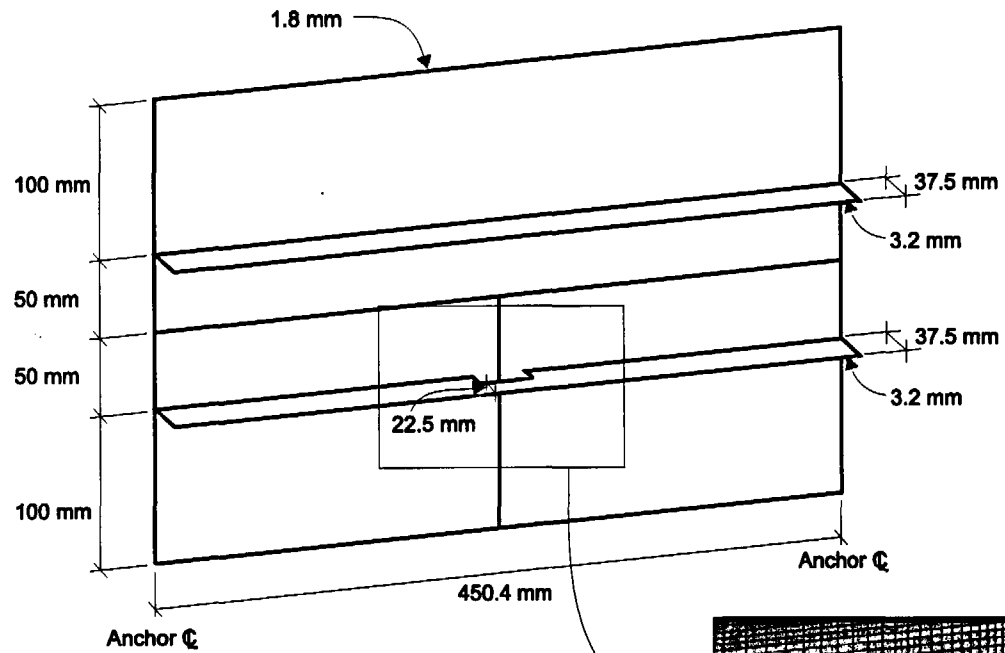


Figure 8-3. Liner Seam Model Geometric Details

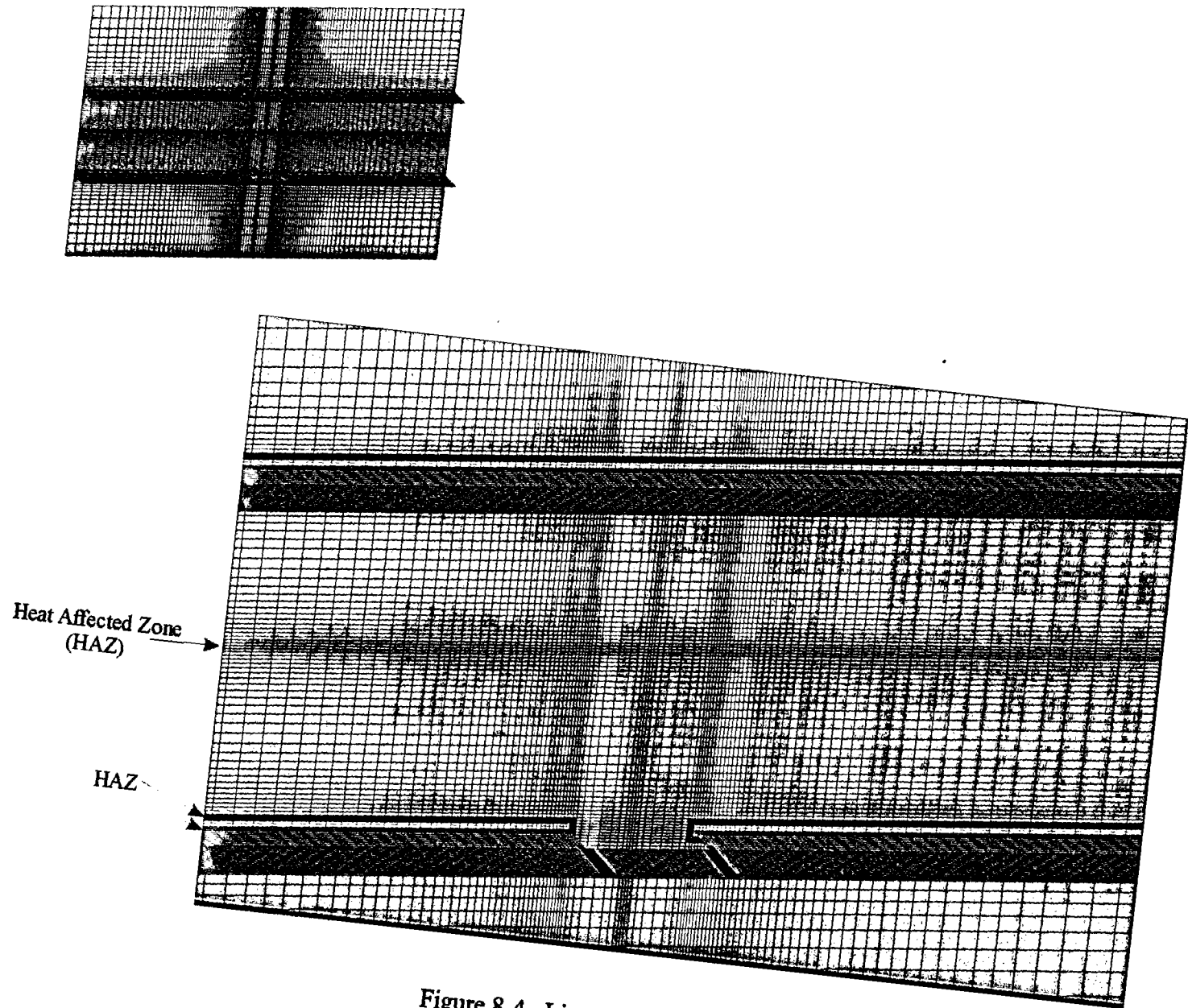


Figure 8-4. Liner Seam Model

PCCV Liner Meridional Strain
135, 6.2 m, Gage LSI-M-Z06-01

291

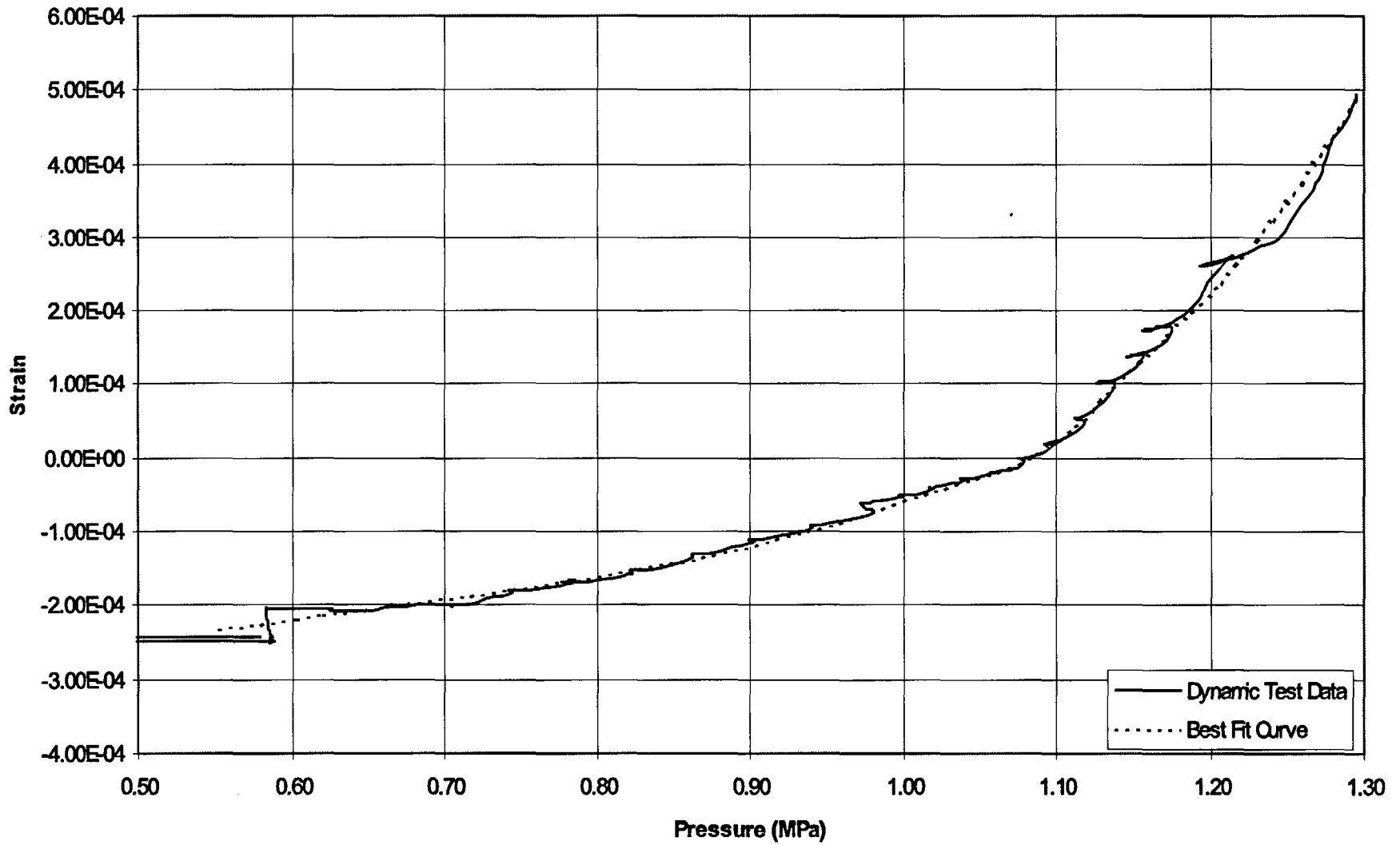


Figure 8-5. PCCV Liner Model 1, Posttest Analysis, Mesh Sensitivity, Measured Liner Meridian Strain at Gage LSI-M-Z6-01 with Best-Fit Curve Liner Model

**PCCV - Radial Displacement
135, 4.68m, Gage DT-R-Z5-01**

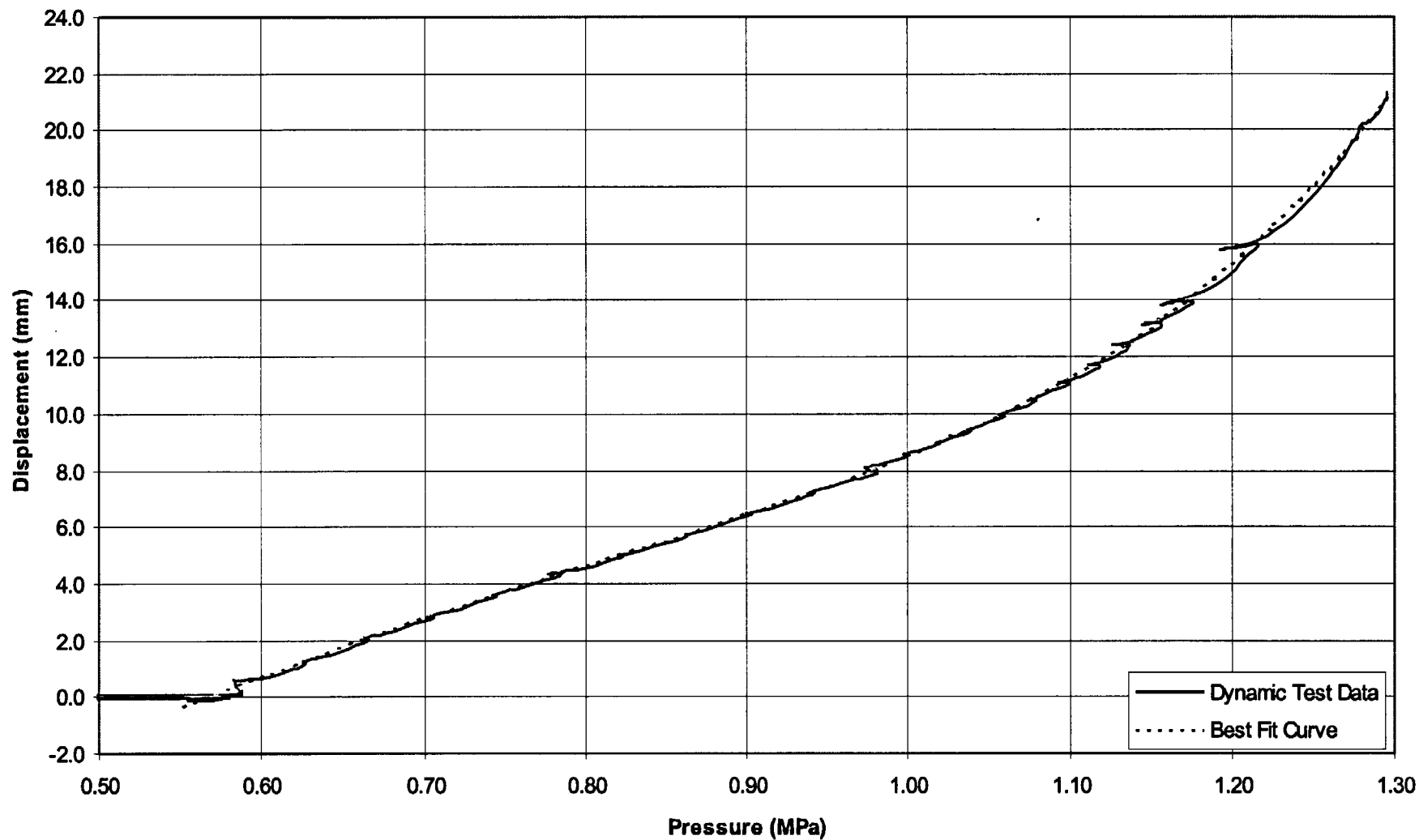


Figure 8-6. PCCV Liner Model 1, Posttest Analysis, Mesh Sensitivity, Measured Liner Radial Displacement at Gage DT-R-Z5-01 with Best-Fit Curve Liner Model

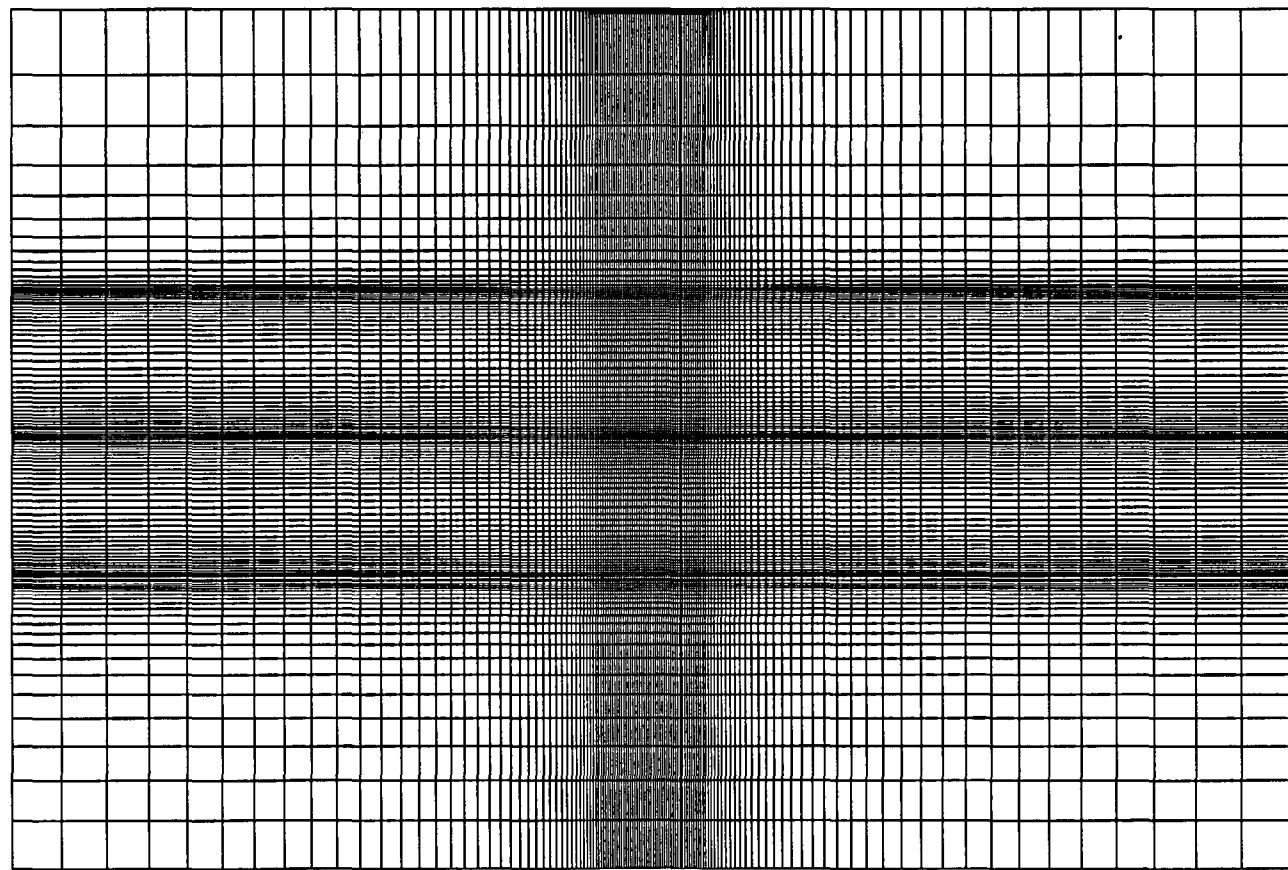
Element	lel 1 = 38	jel 1 = 10	kel 1 = 18	kel 6 = 18
	lel 2 = 11	jel 2 = 10	kel 2 = 2	kel 7 = 15
	lel 3 = 11	jel 3 = 1	kel 3 = 2	kel 8 = 2
	lel 4 = 11		kel 4 = 18	kel 9 = 2
	lel 5 = 11		kel 5 = 18	kel 10 = 14
	lel 6 = 38			

RatHole Lower Stiffener Only



Free Edge

Liner Side



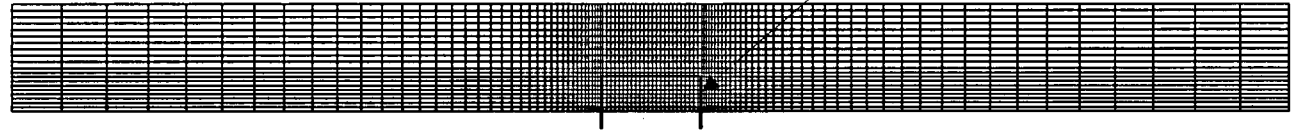
Model Statistics

Nodes 18161
 Elements 17440
 DOF 107772

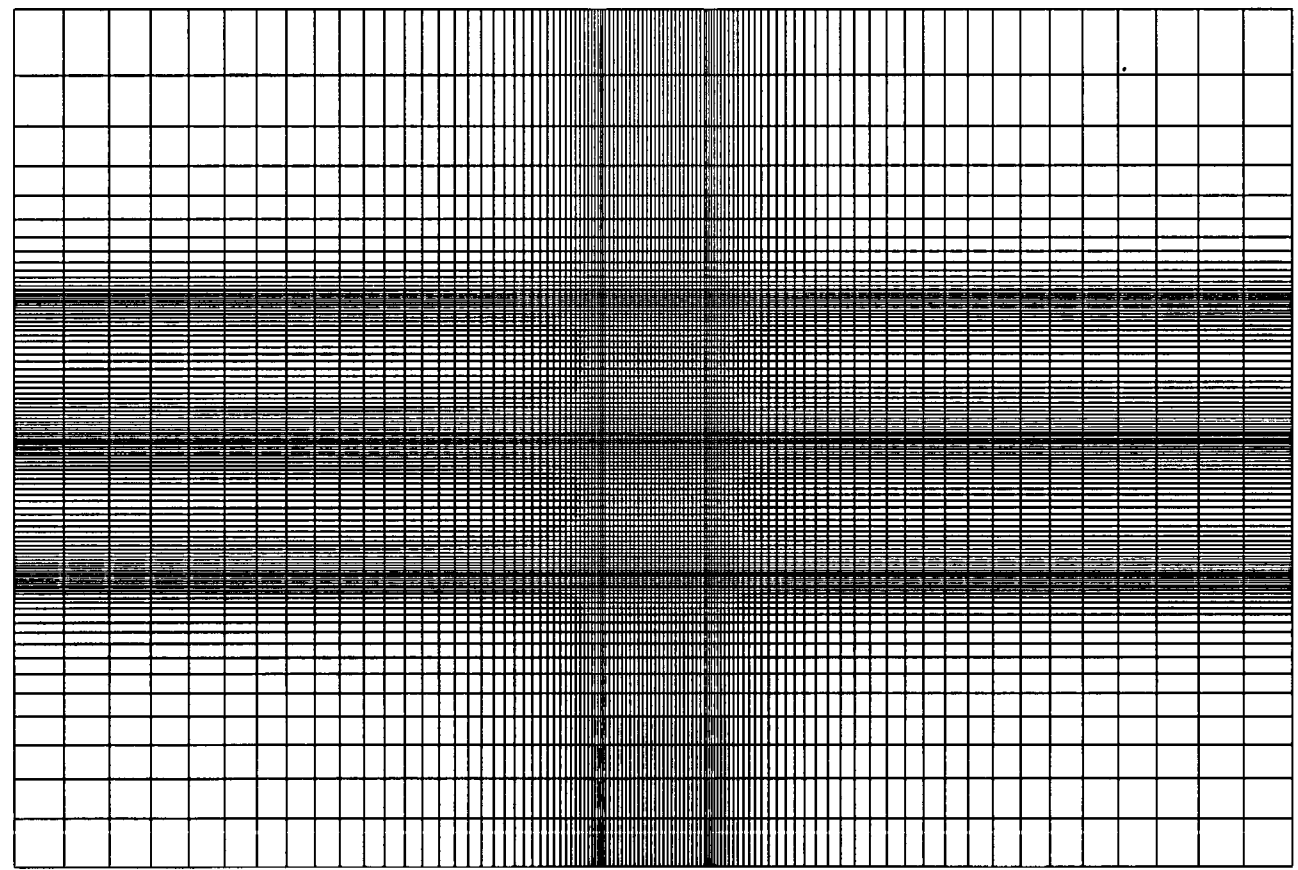
Figure 8-7. PCCV Liner Model 1, Posttest Analysis, Mesh Sensitivity - Baseline Mesh (Model 1)

Element	kel 1 = 38	jel 1 = 10	Kel 1 = 18	Kel 6 = 18
	kel 2 = 6	jel 2 = 10	kel 2 = 2	kel 7 = 15
	kel 3 = 6	jel 3 = 1	kel 3 = 2	kel 8 = 2
	kel 4 = 6		kel 4 = 18	kel 9 = 2
	kel 5 = 6		kel 5 = 18	kel 10 = 14
	kel 6 = 38			

Rathole Lower Stiffener Only



Free Edge
Liner Side

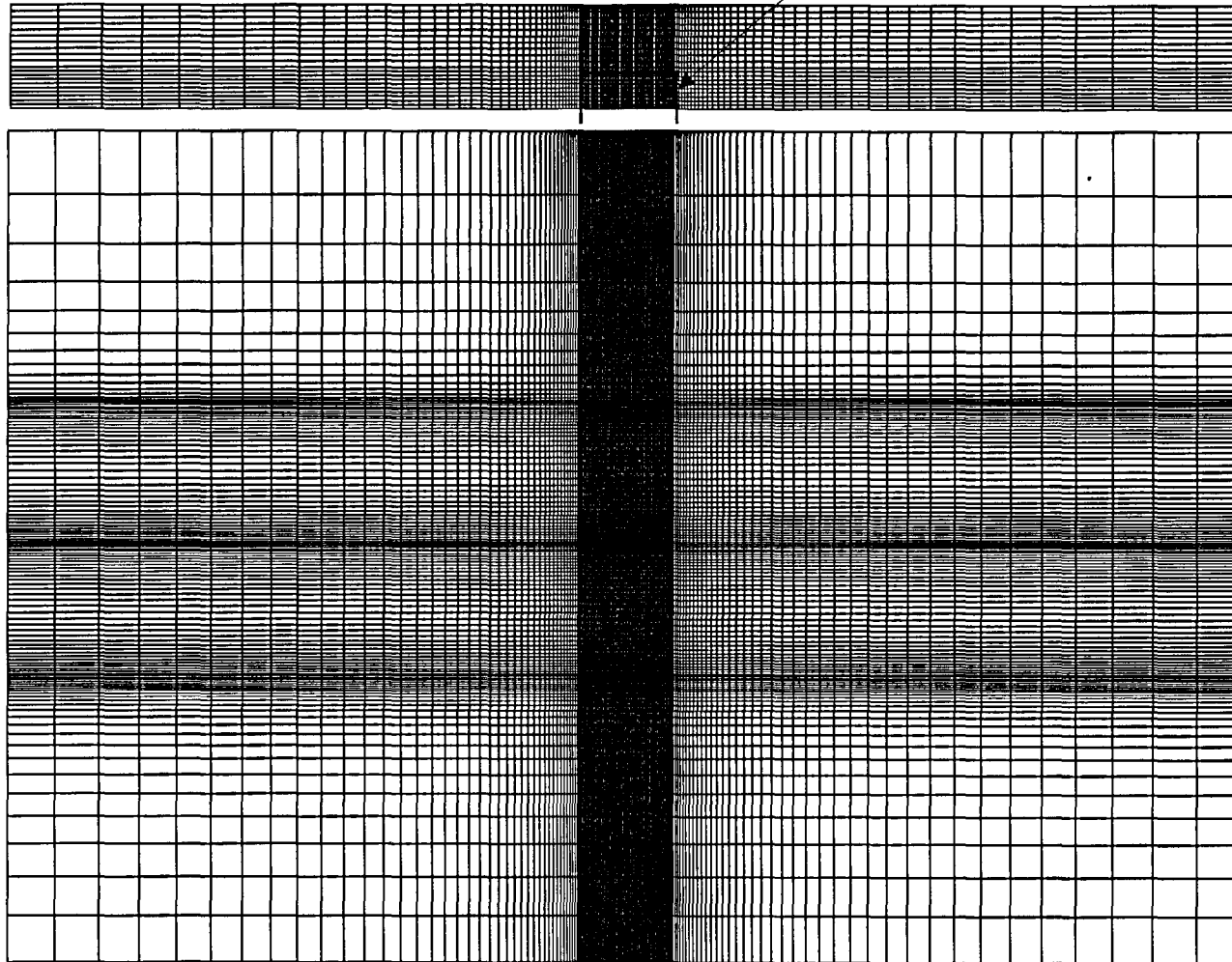


Model Statistics
Nodes 14660
Elements 15301
DOF 90732

Figure 8-8. PCCV Liner Model 2, Posttest Analysis, Mesh Sensitivity - Coarse Mesh

Element	lel 1 = 38	jel 1 = 10	kel 1 = 18	Kel 6 = 18
	lel 2 = 16	jel 2 = 10	kel 2 = 2	kel 7 = 15
	lel 3 = 16	jel 3 = 1	kel 3 = 2	kel 8 = 2
	lel 4 = 16		kel 4 = 18	kel 9 = 2
	lel 5 = 16		kel 5 = 18	kel 10 = 14
	lel 6 = 38			

"Rat Hole" Lower Stiffener Only



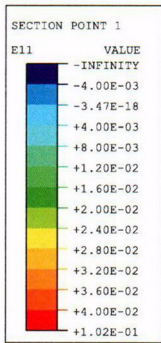
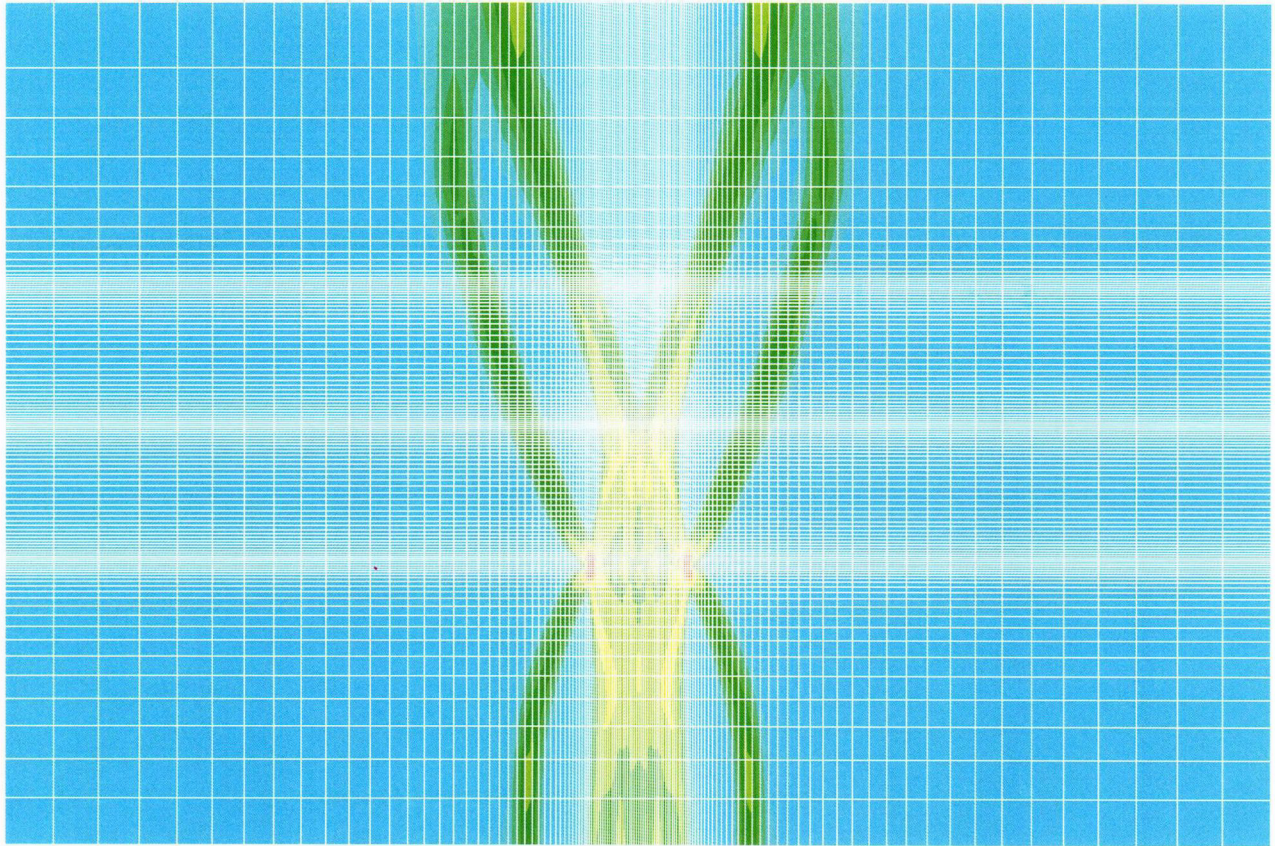
Free Edge

Liner Side

Model Statistics

Nodes 20220
 Elements 21021
 DOF 124812

Figure 8-9. PCCV Liner Model 3, Posttest Analysis, Mesh Sensitivity - Fine Mesh



Enlarged Region Of Liner At Rathole Stiffener Cut Out

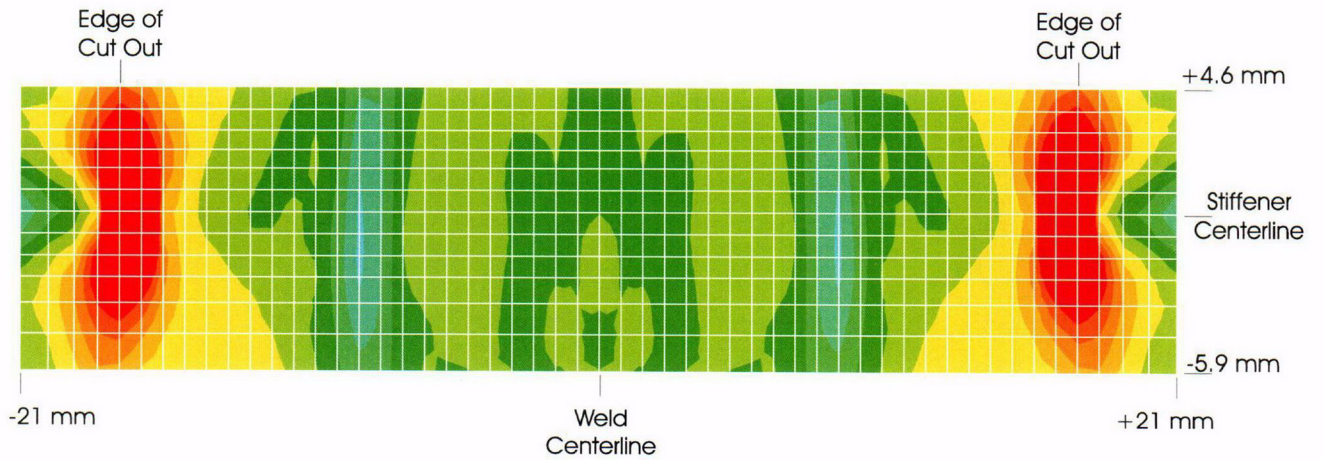
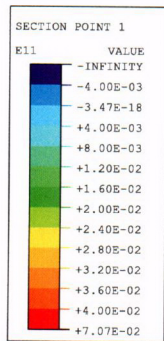
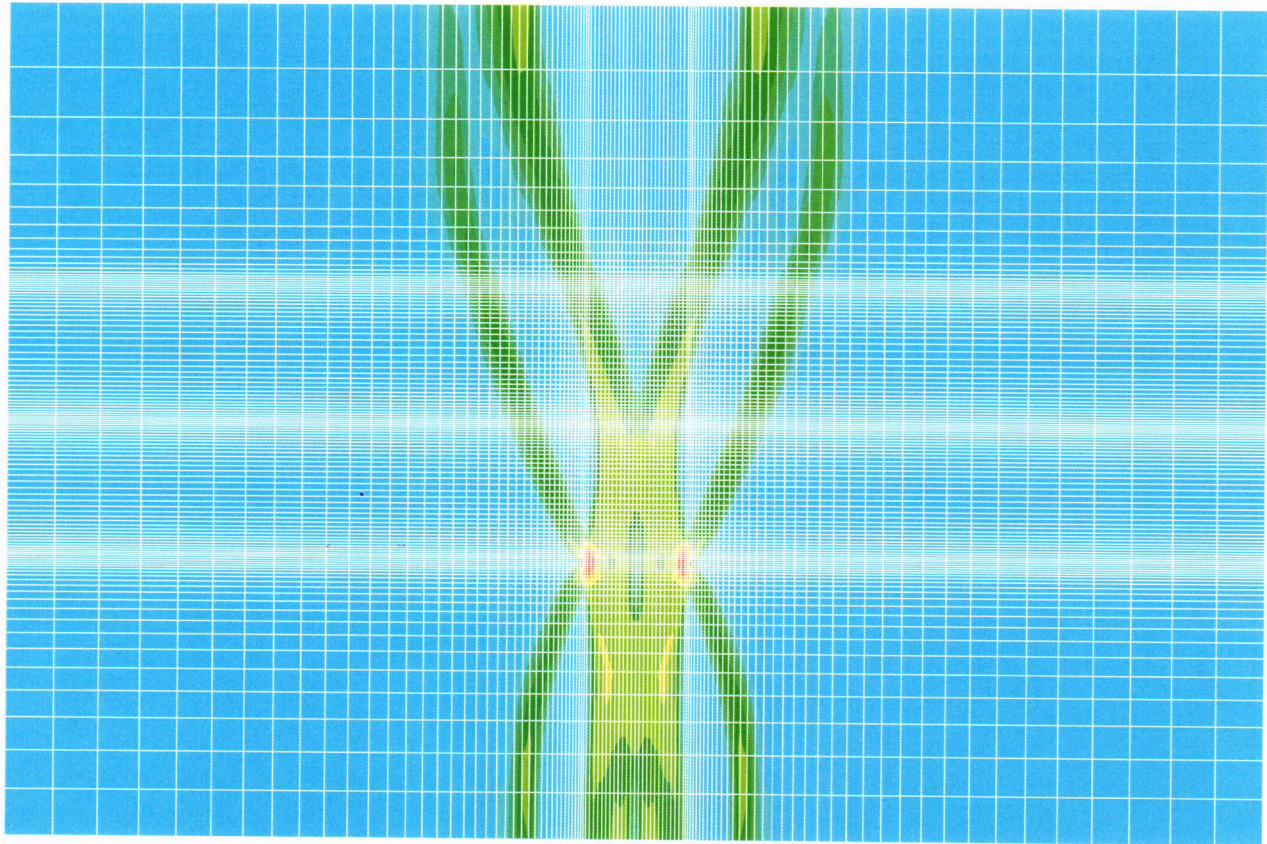


Figure 8-10. PCCV Liner Model 1, Posttest Analysis, Mesh Sensivity, Baseline Mesh, Horizontal Strain Contour Plot At End of Analysis (1.3 MPa)



Enlarged Region Of Liner At Rathole Stiffener Cut Out

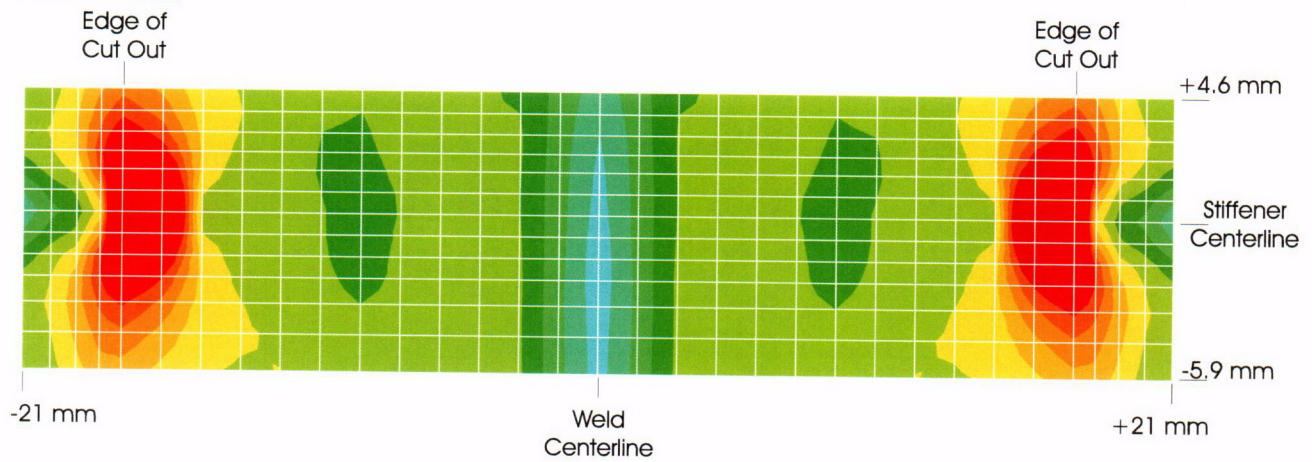
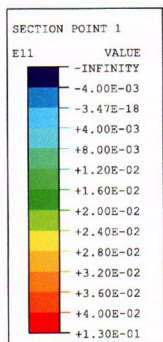
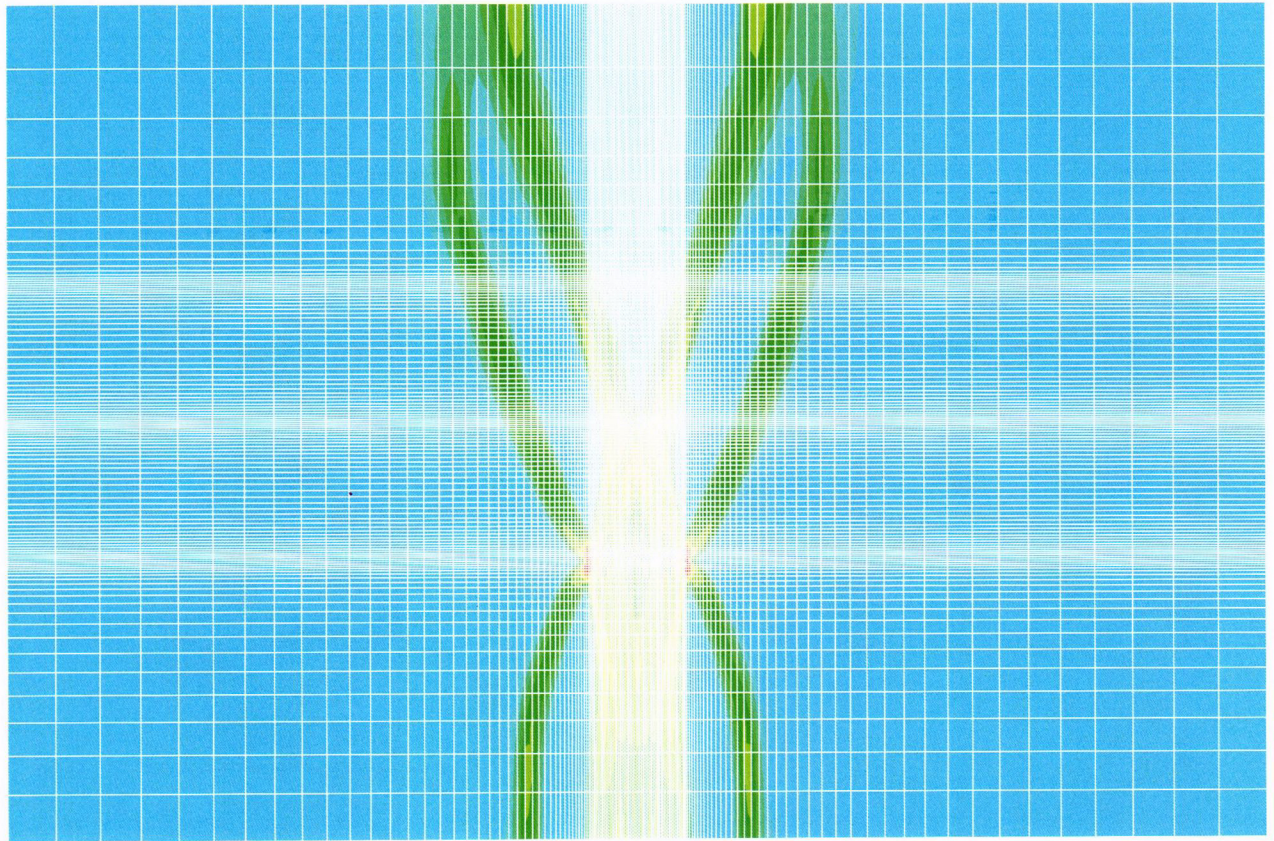


Figure 8-11. PCCV Liner Model 2, Posttest Analysis, Mesh Sensivity, Coarse Mesh, Horizontal Strain Contour Plot At End of Analysis (1.3 MPa)



Enlarged Region Of Liner At Rathole Stiffener Cut Out

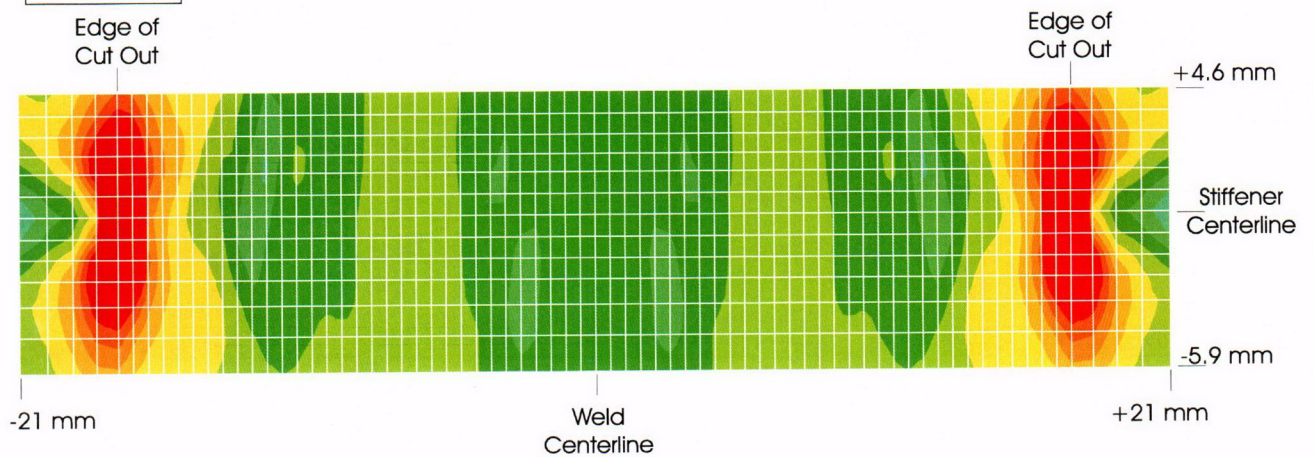


Figure 8-12. PCCV Liner Model 3, Posttest Analysis, Mesh Sensivity, Fine Mesh, Horizontal Strain Contour Plot At End of Analysis, (1.3 MPa)

PCCV - Post-Test, Local Liner Weld-Seam / Rathole Analysis

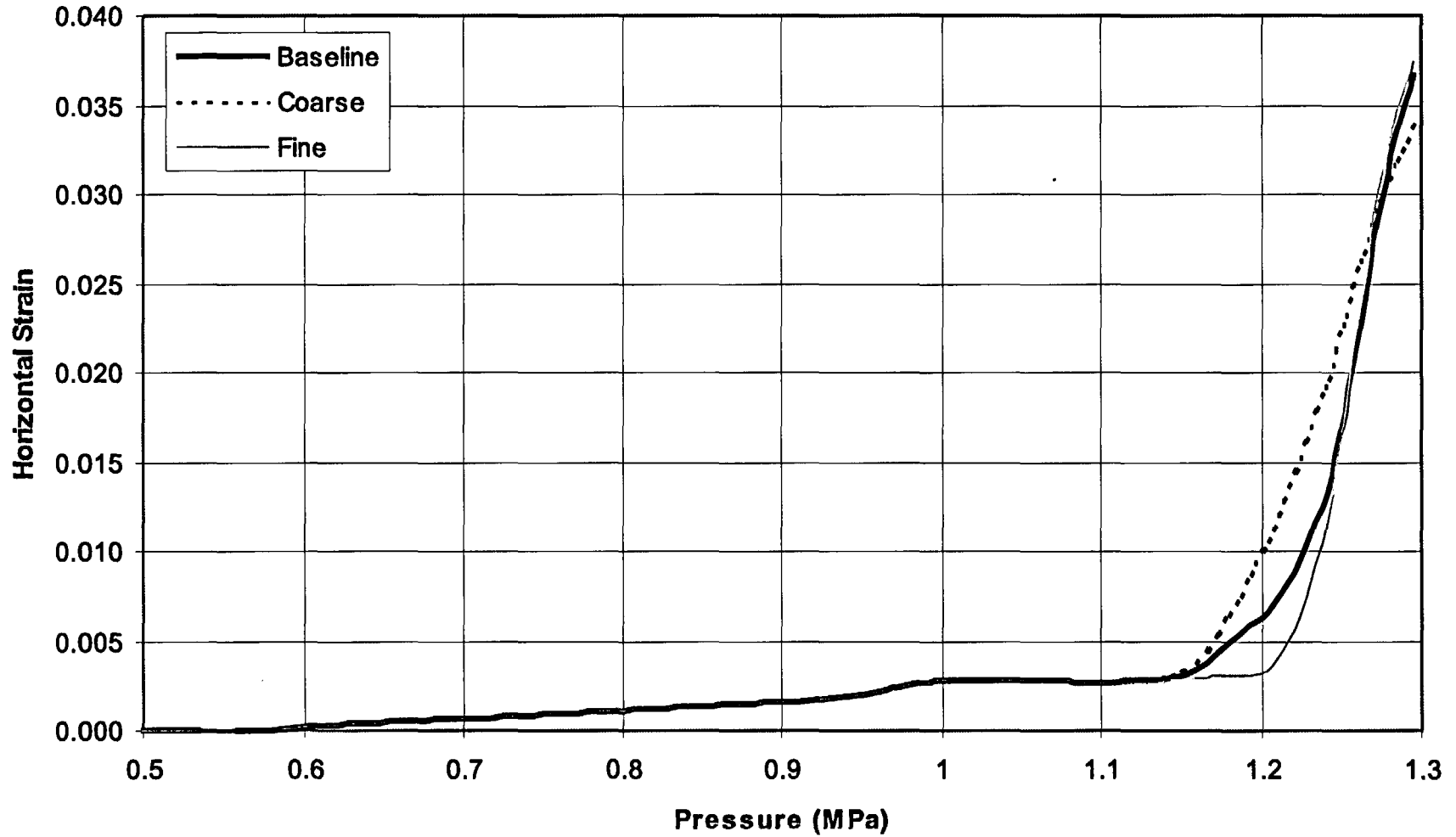


Figure 8-13. PCCV Liner Model, Posttest Analysis, Mesh Sensitivity, Comparison of Horizontal Strain, 5 mm Below Stiffener Reentrant Corner at Rat-Hole

PCCV - Post-Test, Local Liner Weld-Seam / Rathole Analysis

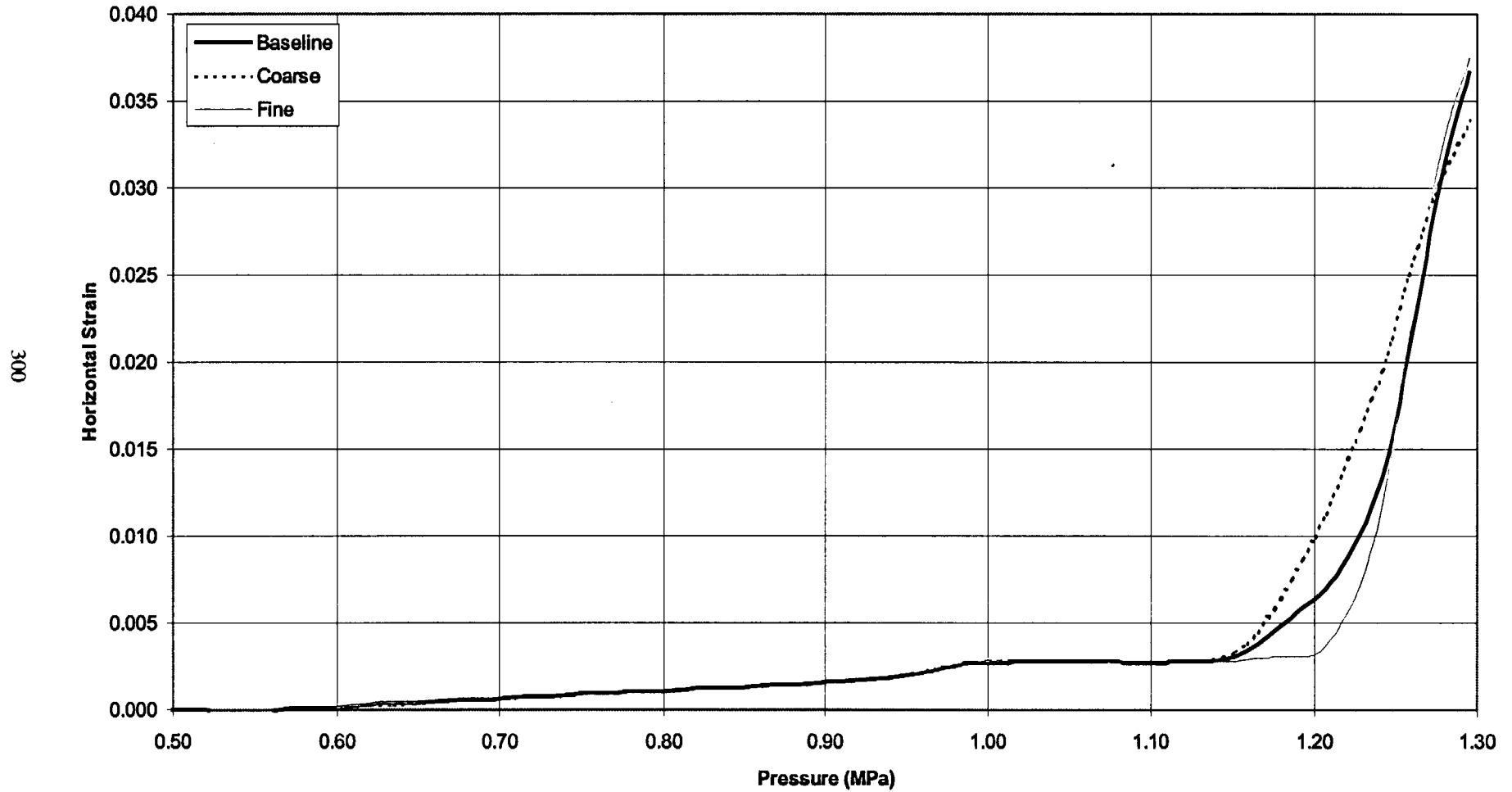


Figure 8-14. PCCV Liner Model, Posttest Analysis, Mesh Sensitivity, Comparison of Horizontal Strain, 1.2 mm Below Stiffener Reentrant Corner at Rat-Hole

PCCV - Post-Test, Local Liner Weld-Seam/Rathole Analysis

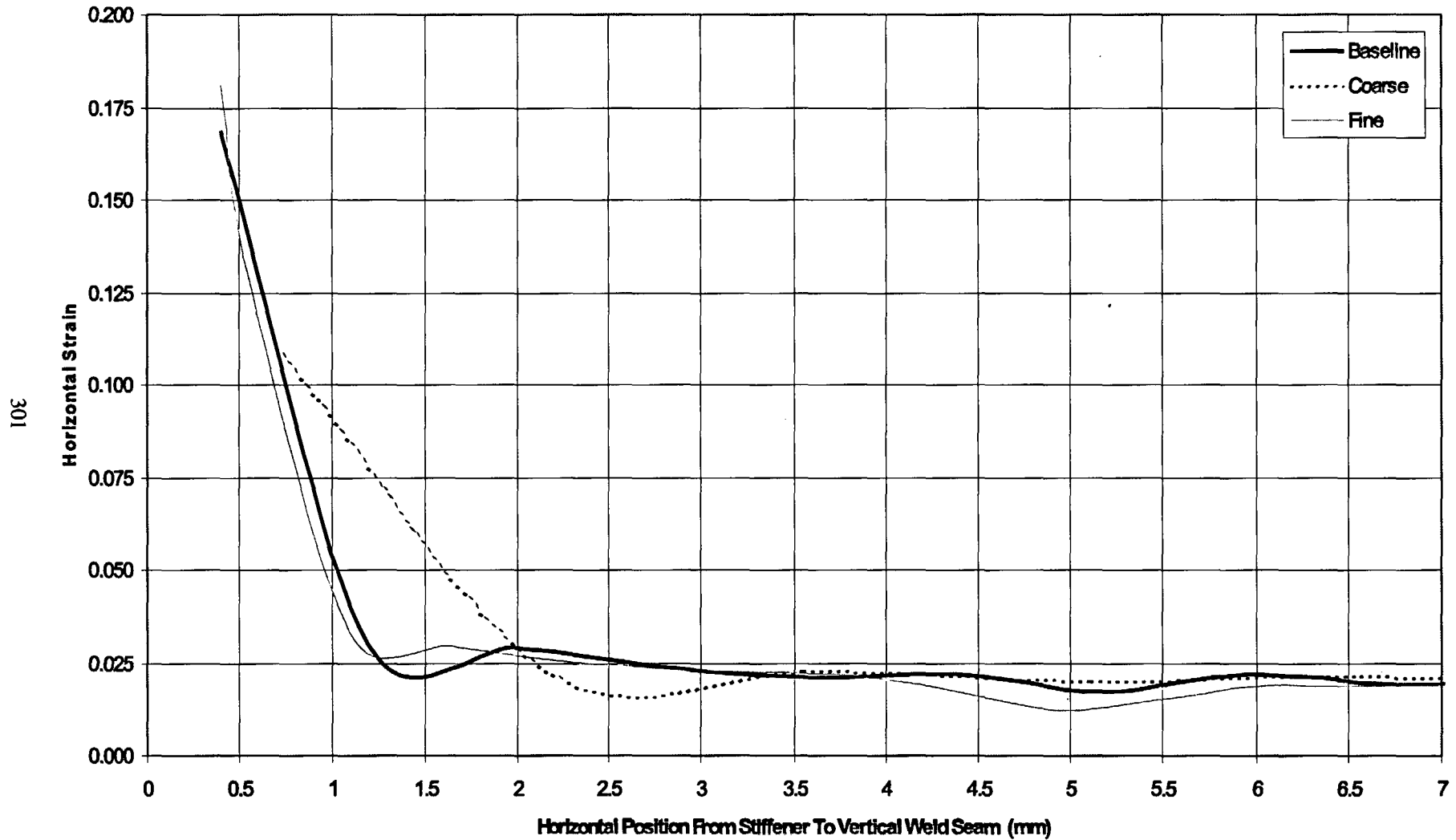
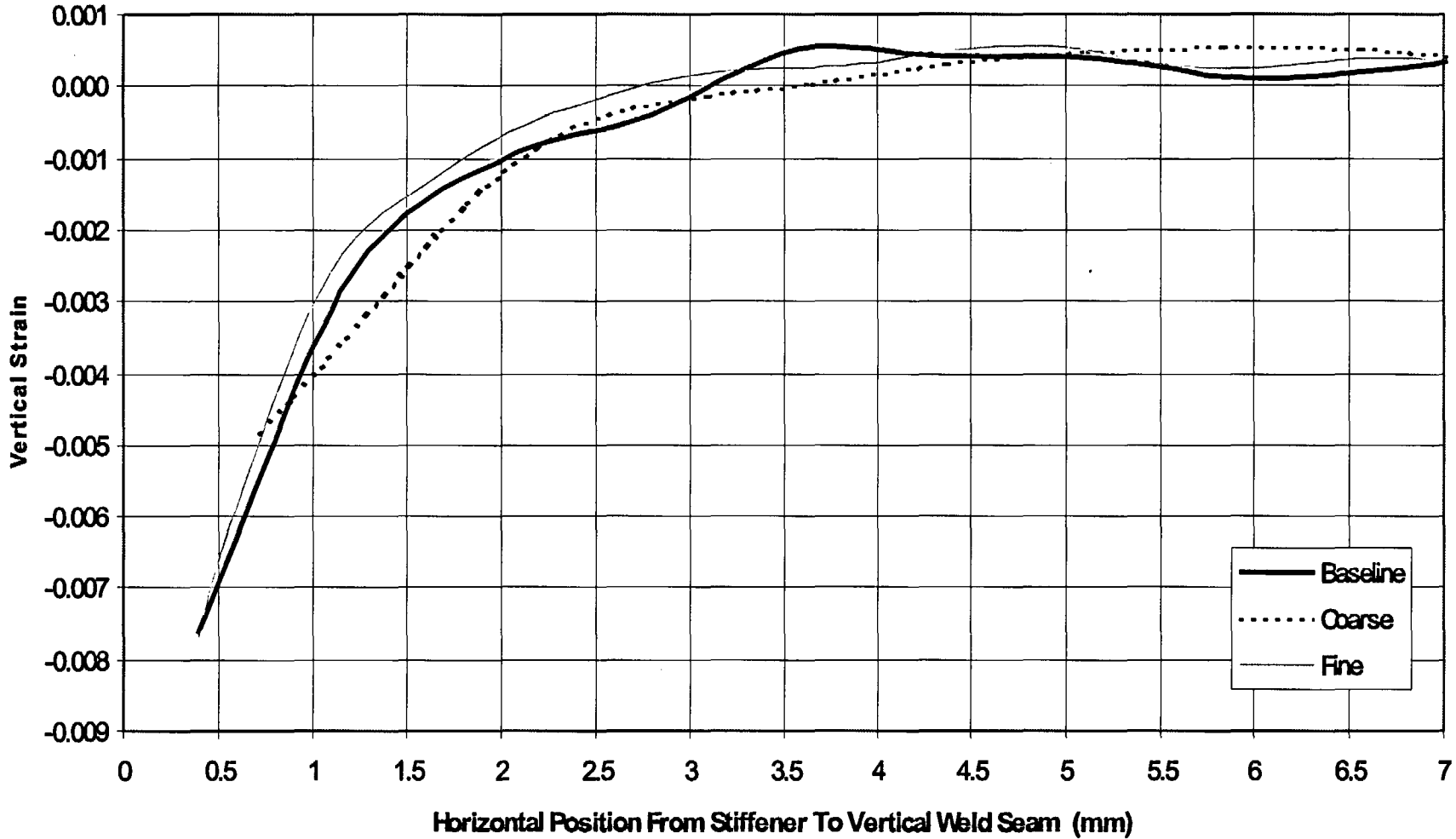


Figure 8-15. PCCV Liner Model, Posttest Analysis, Mesh Sensitivity, Comparison of Horizontal Strains, Horizontal Profile From Stiffener Towards Vertical Weld Seam at P = 1.3 MPa

PCCV - Post-Test, Local Liner Weld-Seam / Rathole Analysis



302

Figure 8-16. PCCV Liner Model, Posttest Analysis, Mesh Sensitivity, Comparison of Vertical Strains, Horizontal Profile from Stiffener Towards Vertical Weld Seam at P = 1.3 MPa

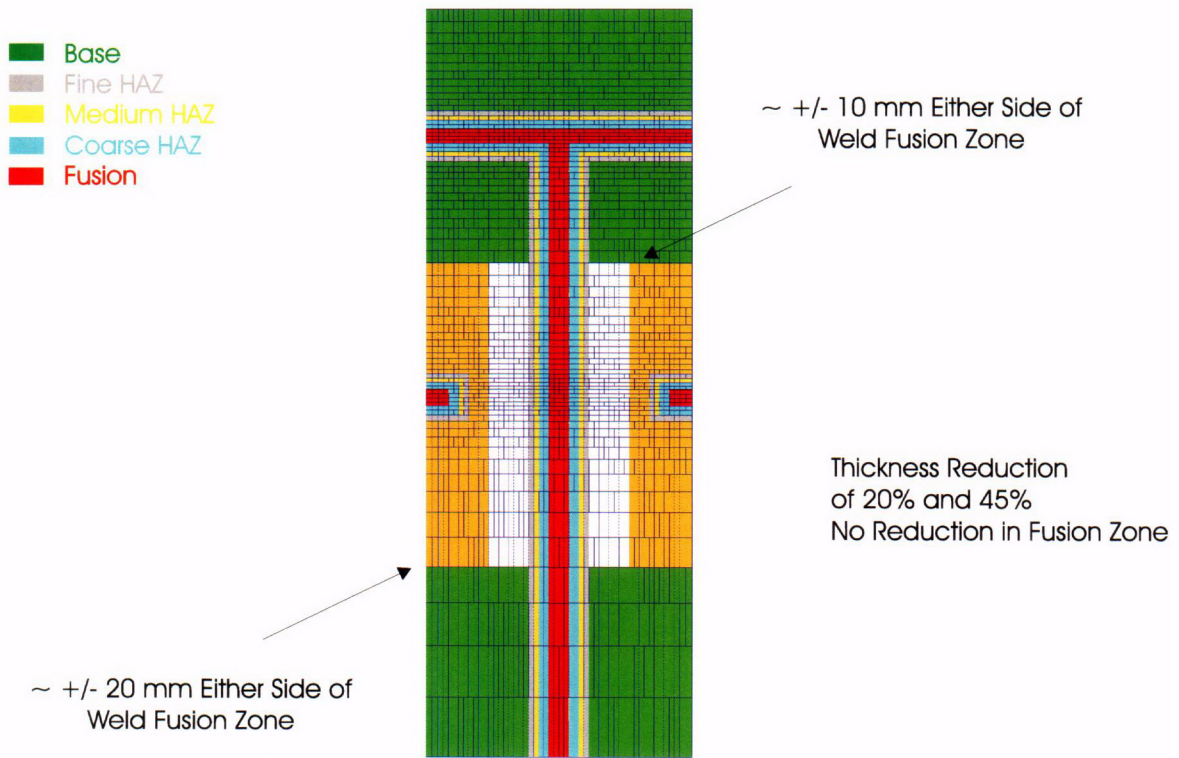
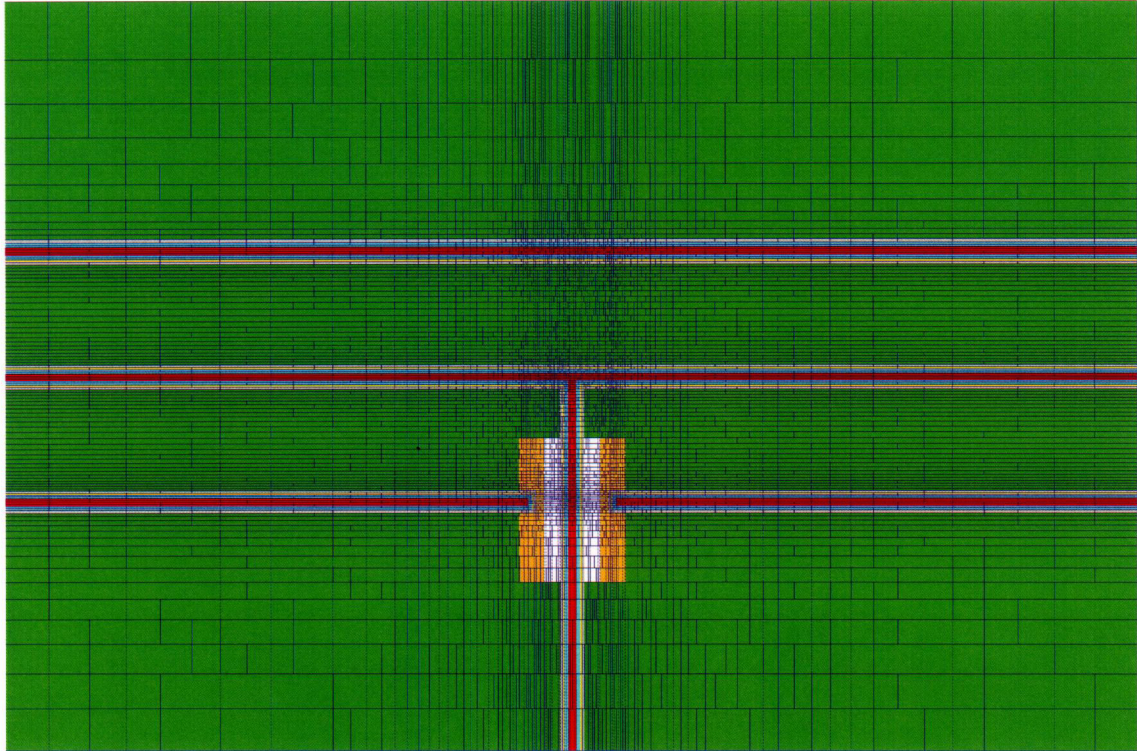
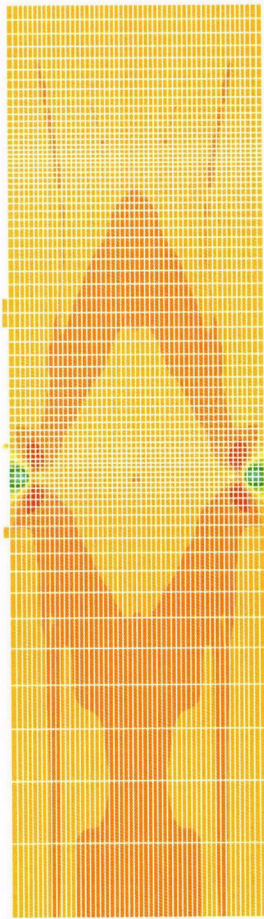
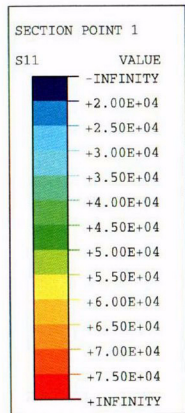
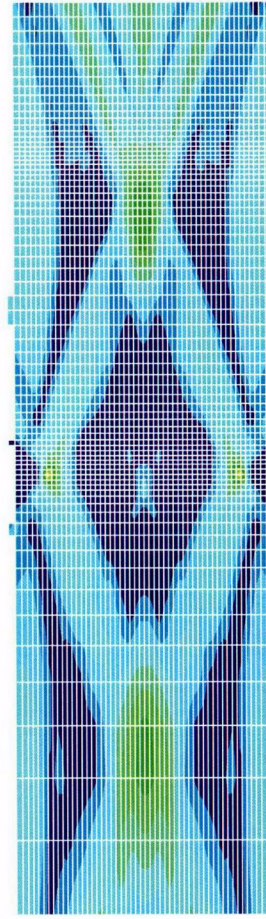
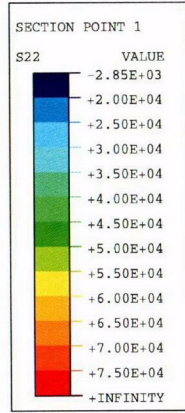


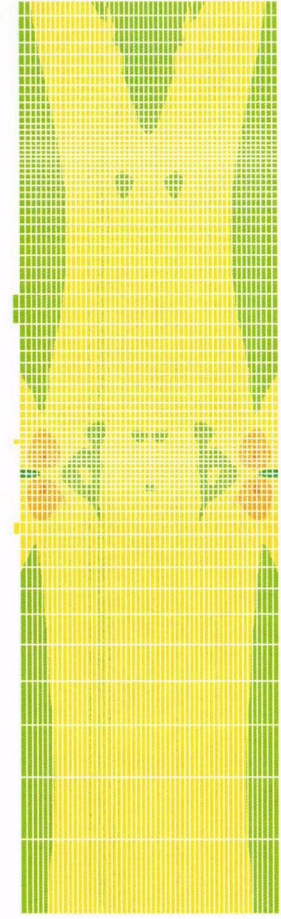
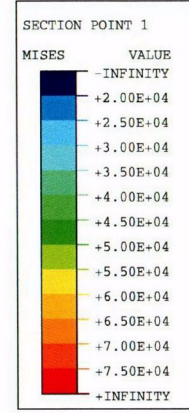
Figure 8-17. PCCV Liner Model, Posttest Analysis, Base, HAZ, and Fusion Regions, Extent of Thinning Zones



Horizontal Stress

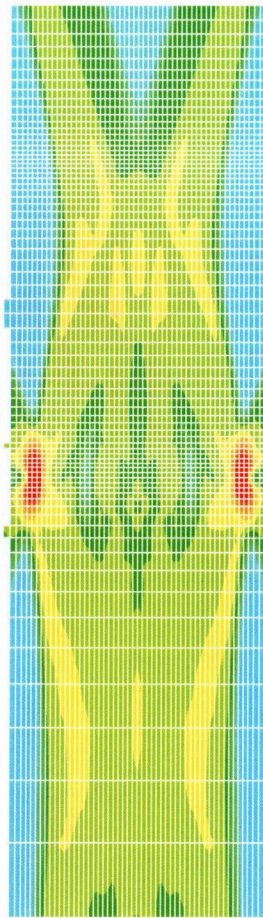
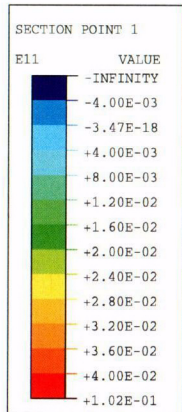


Vertical Stress

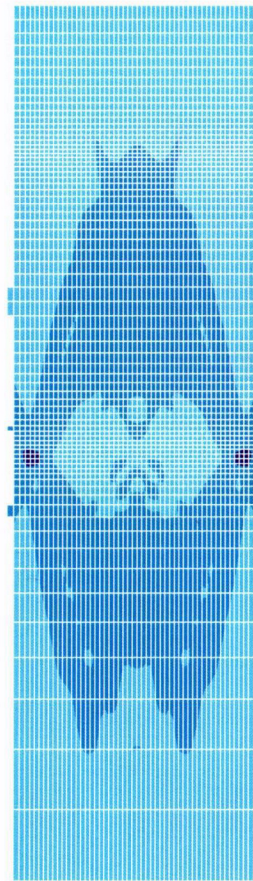
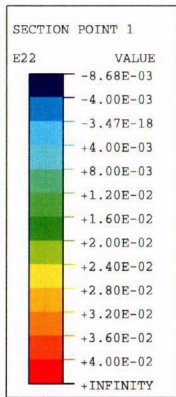


Mises Stress

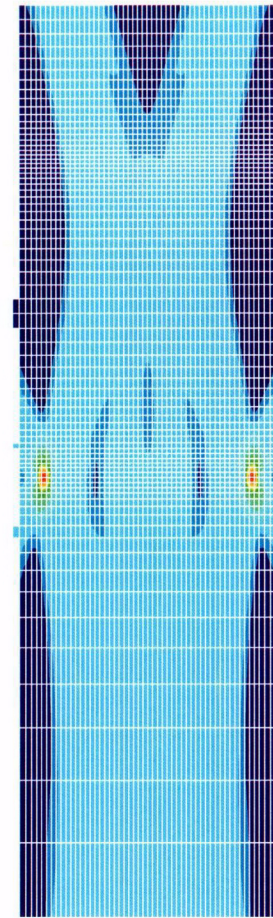
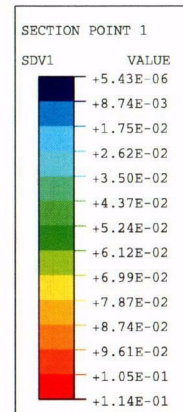
Figure 8-18. PCCV Liner Model, Posttest Analysis, Case 1, Stress Contour, at P = 3.3 Pd
(Stresses in psi; multiply by 0.00690 for MPa)



Horizontal Strain

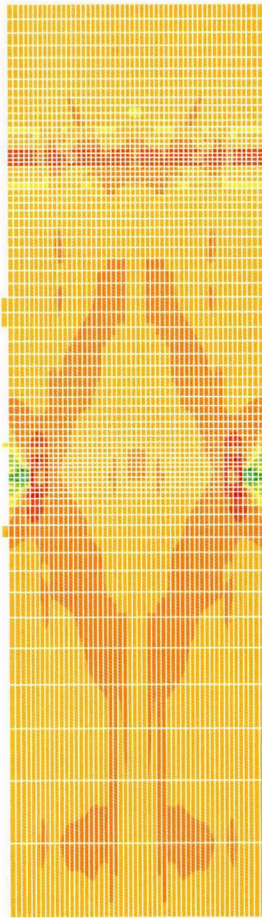
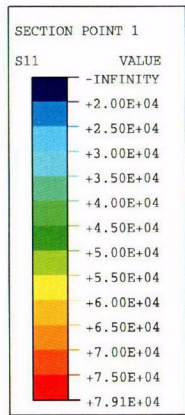


Vertical Strain

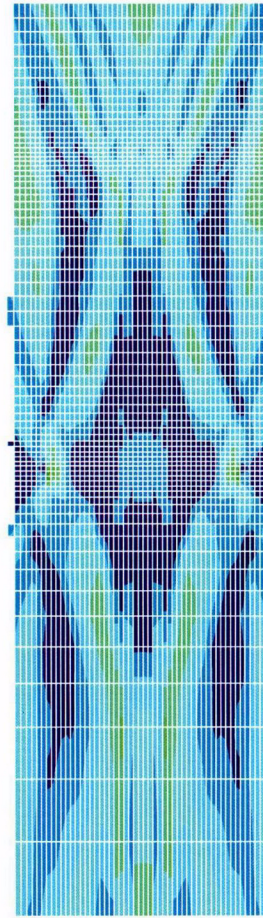
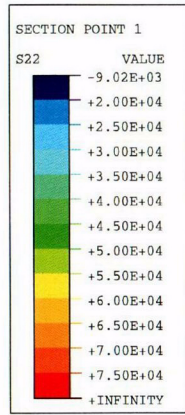


Effective Plastic Strain

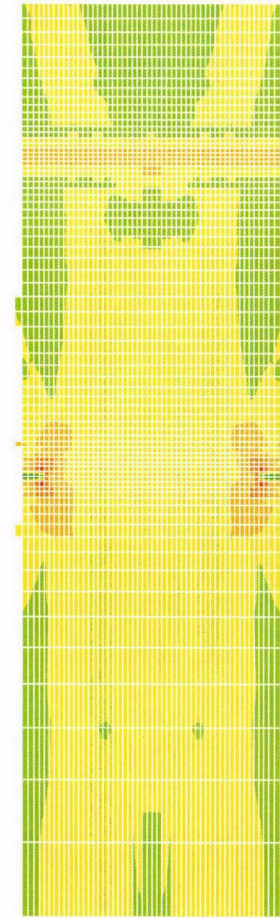
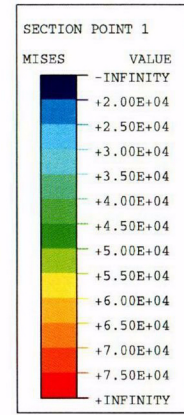
Figure 8-19. PCCV Liner Model, Posttest Analysis, Case 1, Strain Contour, at P = 3.3 Pd



Horizontal Stress

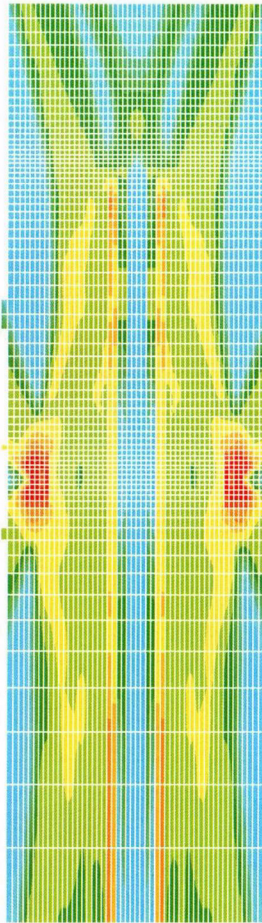
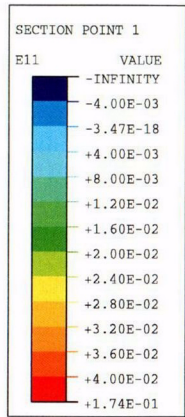


Vertical Stress

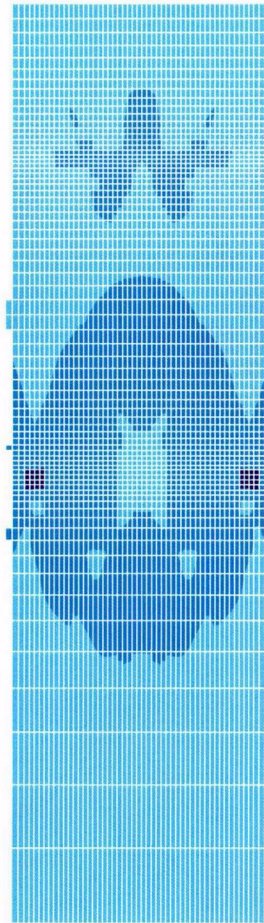
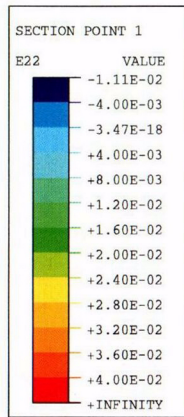


Mises Stress

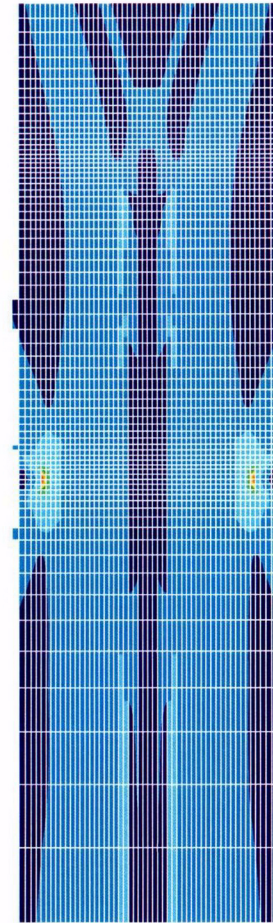
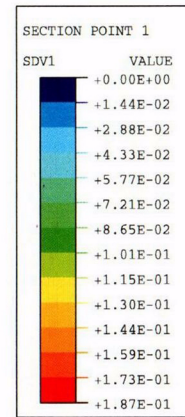
Figure 8-20. PCCV Liner Model, Posttest Analysis, Case 4, Stress Contour, at P = 3.3 Pd
(Stresses in psi; multiply by 0.00690 for MPa)



Horizontal Strain

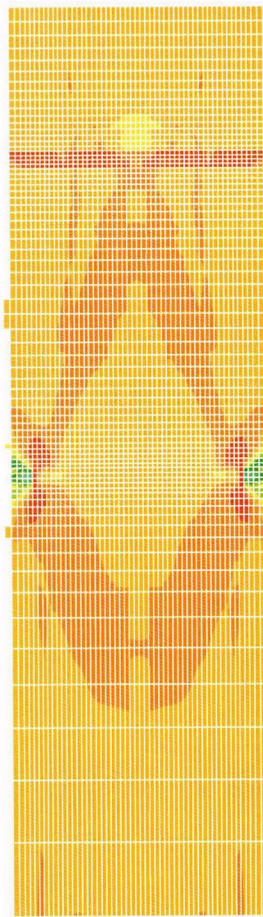
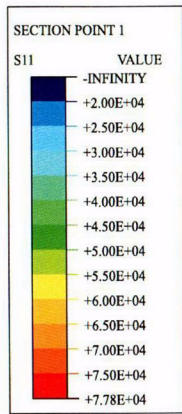


Vertical Strain

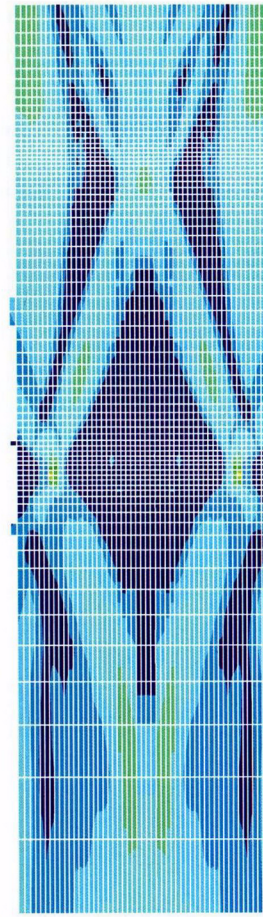
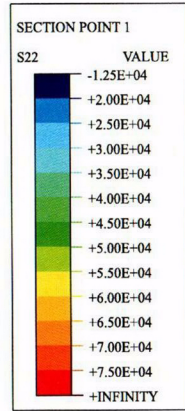


Effective Plastic Strain

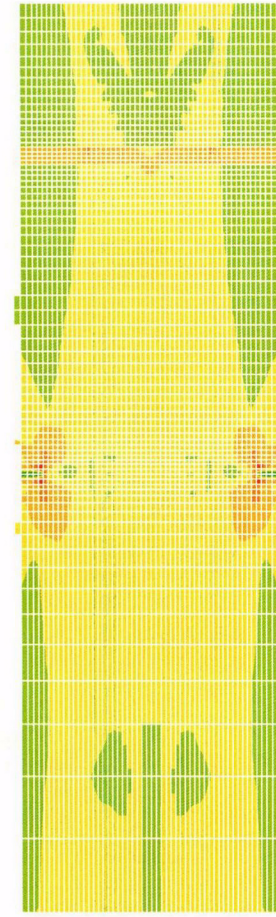
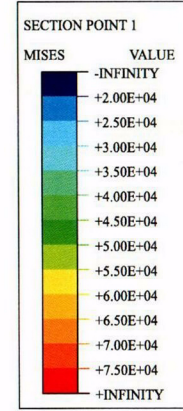
Figure 8-21. PCCV Liner Model, Posttest Analysis, Case 4, Strain Contour, at P = 3.3 Pd



Horizontal Stress



Vertical Stress



Mises Stress

Figure 8-22. PCCV Liner Model, Posttest Analysis, Case 5, Stress Contour, at P = 3.3 Pd
(Stresses in psi; multiply by 0.00690 for MPa)